causing genetic diseases (18). Disease-causing mutations also affect the first nucleotide of an exon (E^{+1}), but their effects on pre-mRNA splicing have been rarely scrutinized. As far as we know, only three such mutations in *FECH* (19), *GH1* (20) and *EYA1* (21) have been reported to cause aberrant splicing. Similarly, two such mutations in *LPL* (22) and *HEXA* (23) have been reported to have no effect on splicing. In this communication, we dissected molecular bases that differentiate splicing-disrupting and splicing-competent mutations, and found that AG-dependent ss is vulnerable to a mutation at E^{+1}, whereas AG-independent ss is tolerant.

MATERIALS AND METHODS

Minigene constructs and mutagenesis

Human genes of our interest were PCR-amplified from HEK293 cells using the KOD plus DNA polymerase (Toyobo). We introduced restriction enzyme-recognition sites at the 5′-end of the forward and reverse primers. We inserted the amplicon into the pcDNA3.1(+) mammalian expression vector (Invitrogen). We introduced patients' or artificial mutations with the QuikChange site-directed mutagenesis kit (Stratagene). We confirmed the absence of unexpected artifacts with the CEQ8000 genetic analyzer (Beckman Coulter).

Cell culture and transfection procedures

HEK293 cells were maintained in the Dulbecco's minimum essential medium (DMEM, Sigma-Aldrich) with 10% fetal bovine serum (FBS, Sigma-Aldrich). At ~50% confluency (~5×10^5 cells) in a 12-well plate, 1 ml of fresh Opti-MEM I (Invitrogen) was substituted for DMEM, and 500 ng of a minigene with 1.5 µl of the FuGENE6 transfection reagent (Roche Diagnostics) were then added. After 4 h, 2 ml of DMEM with 10% FBS was overlaid, and the cells were incubated overnight. The transfection medium was replaced with 2 ml of fresh DMEM with 10% FBS. RNA was extracted at 48 h after initiation of transfection.

RNA extraction and RT–PCR

Total RNA from HEK293 was extracted by Trizol reagent (Invitrogen) according to the manufacturer's protocols. The quantity and quality of RNA was determined by spectrophotometry (NanoDrop Techonologies). Twenty percent of the isolated RNA was used as a template for cDNA synthesis with the Oligo(dT) 12–18 Primer (Invitrogen) and the ReverTra Ace (Toyobo). Ten percent of the synthesized cDNA was used as a template for RT–PCR amplification with T7 primer (5′-TAATACG ACTCACTATAGGG-3′) and gene-specific primers for minigenes in pcDNA3.1(+). Image J software (National Institutes of Health) was used to quantify intensities of fragments. We employed JMP (SAS Institute) for statistical analysis.

RNA interference to knockdown U2AF^{35}

We synthesized siRNA of 5′-GGCUGUGAUUGACUU GAAUdTdT-3′ (GenBank accession number NM_006758, nucleotides 459–479), which is against the shared sequence of U2AF^{35}a and U2AF^{35}b (15). We employed Lipofectamine 2000 (Invitrogen) to cotransfect plasmids and siRNAs according to the manufacturer's protocols. Briefly, the transfection reagent included 300 ng of the plasmid, 50 pmol of siRNA, and 2 µl of lipofectamine 2000 in 100 µl of Opti-MEM I. The cells were harvested by western blotting for 48 h after transfection. The primary antibodies were goat polyclonal antibody for U2AF^{35} (Santa Cruz Biotechnology), and mouse monoclonal antibodies for U2AF^{65} (Santa Cruz Biotechnology) and PTB (Zymed Laboratories). The secondary antibodies were HRP-conjugated mouse anti-goat (Santa Cruz Biotechnology) or sheep anti-mouse (GE healthcare) antibodies. The immunoreactive proteins were detected by enhanced chemiluminescence (ECL, Amersham Biosciences).

For the siRNA rescue assay, we cloned the human U2AF^{35} cDNA (Open Biosystems) into the HindIII and EcoRI restriction sites of the p3XFLAG-CMV-14 vector (Sigma-Aldrich). We introduced four silent mutations into the siRNA target region using the QuikChange site-directed mutagenesis kit with a primer, 5′-GAAAAG GCTGTAATCGATTTAAATAACCGTTGGTT-3′, where artificial mutations are underlined (24).

RNA probe synthesis

We synthesized [α-^{32}P]-CTP-labeled RNA using the Riboprobe *in vitro* transcription system (Promega) from a PCR-amplified fragment according to the manufacturer's instructions. We used the same forward primer for all the probes with the sequence of 5′-*TAATACGACTCACT ATAGG*GAGACAGG-3′, where the italicized is T7 promoter and the underlined is for annealing to the reverse primer. The four reverse primers were: wild-type *FECH*, 5′-TGGACCAACCTATGCGAAAGATAGACG AATGCGTAAGCCTGTCTC-3′; mutant *FECH*, 5′-TGG ACCAAACTATGCGAAAGATAGACGAATGCGTA AGCCTGTCTC-3′; wild-type *LPL*, 5′-TGGATCGAGG CCTTAAAAGGGAAAAAAGCAGGAACACCCTGT CTC-3′; and mutant *LPL*, 5′-TGGATCGAGGACTTAA AAGGGAAAAAAGCAGGAACACCCTGTCTC-3′, where the underlined is for annealing to the forward primer.

Expression and purification of recombinant proteins

The human U2AF^{35} and U2AF^{65} cDNAs were obtained from Open Biosystems. U2AF^{35} and U2AF^{65} cDNAs were subcloned into the *Bam*HI and *Eco*RI restriction sites of the pFastBac HTb vector. The recombinant baculoviruses were expressed using the Bac-to-Bac Baculovirus Expression System (Invitrogen) according to the manufacturer's instructions. Infected Sf9 cells were harvested after 48 h and resuspended in the lysis buffer containing 50 mM sodium phosphate, 10 mM imidazole, 300 mM NaCl, 1% Triton X-100, 2 mM

β-mercaptoethanol, the Complete Protease Inhibitor Cocktail (Roche Applied Science) and 5 U endonuclease in pH 7.0. His-tagged U2AF^{35} and U2AF^{65} proteins were purified using the TALON metal affinity resins (Clontech) under the denatured and native conditions, respectively. Purified U2AF^{35} was refolded by extended dialysis in dialysis buffer (50 mM sodium phosphate, 300 mM NaCl, 150 mM imidazole, pH 7.0). We determined the protein concentrations using the Pierce 660 nm Protein Assay Reagent (Thermo Scientific).

RNA-electrophoretic mobility shift assay

The radioactively labeled RNA (1×10^5 cpm) was incubated at room temperature with varying concentrations of recombinant proteins, 16 μg of yeast tRNA, and 1.6 U of RNasin (Toyobo) in a final volume of 20 μl of the binding buffer (20 mM HEPES pH 7.8, 50 mM KCl, 3 mM $MgCl_2$, 0.5 mM dithiothreitol, 0.5 mM EDTA and 5% glycerol). After 20 min, the RNA–protein complexes were separated on 5% non-denaturing polyacrylamide gels in 1 × TBE buffer at 4°C. The gels were dried and complex formation was visualized using the Typhoon 8600 Imager (GE Healthcare).

In silico analysis of the human genome and ESE-motifs

We analyzed human genome annotations (NCBI Build 37.1, hg19) by writing Perl programs, and executing them either on the PrimePower HPC2500/Solaris 9 supercomputer (Fujitsu) or on the cygwin UNIX emulator running on a Windows computer. To search for ESE-motifs, we used the ESE Finder (http://rulai.cshl.org/ESE/) (25,26), the RESUCE-ESE server (http://genes.mit.edu/burgelab/rescue-ese/) (27), the FAS-ESS server (http://genes.mit.edu/fas-ess/) (28), the PESX server (http://cubweb.biology.columbia.edu/pesx/) (29,30), and the ESRsearch server (http://ast.bioinfo.tau.ac.il/) (31).

RESULTS

Recapitulation of normal and aberrant splicing in minigenes

We first constructed minigenes of *GH1*, *FECH*, *EYA1*, *LPL* and *HEXA*, and introduced a previously reported disease-causing mutation at E^{+1} (Figure 1A). These minigenes successfully recapitulated normal and aberrant splicings: mutations in *GH1*, *FECH* and *EYA1* caused exon skipping, whereas those in *LPL* or *HEXA* did not (Figure 1B).

Down-regulation of U2AF^{35} increased exon skipping in wild-type *GH1* and *FECH*, but not in wild-type *EYA1*, *LPL* and *HEXA*

We predicted that a mutation at E^{+1} should disrupt binding of U2AF^{35}. We thus hypothesized that *GH1*, *FECH* and *EYA1* require binding of U2AF^{35} for the assembly of spliceosome, whereas *LPL* and *HEXA* do not require it. To prove this hypothesis, we first knocked down U2AF^{35} and analyzed its effect on the wild-type minigenes. We achieved an efficient down-regulation of U2AF^{35} in HEK293 cells (Figure 2A). We also confirmed

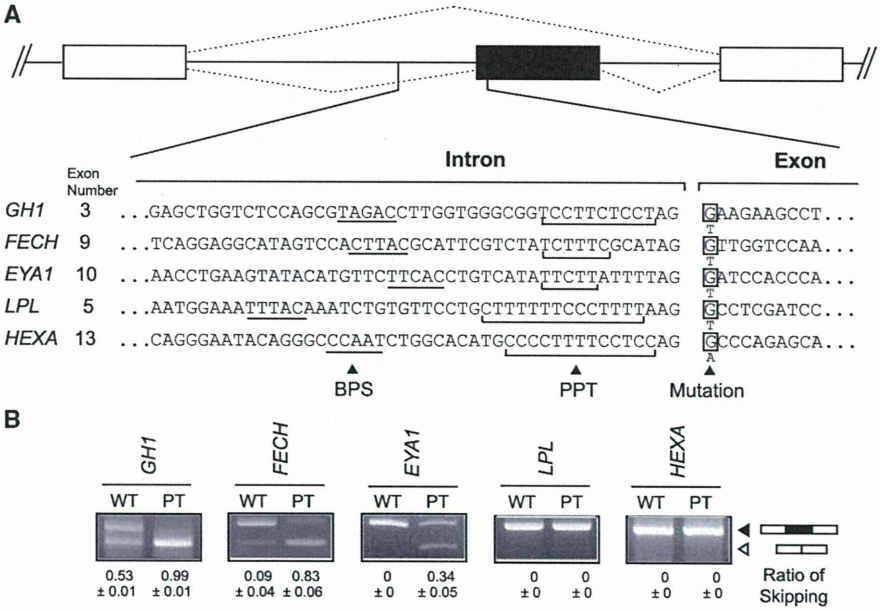

Figure 1. Recapitulation of normal and aberrant splicing of five genes. (**A**) Nucleotide sequences at the intron/exon junctions of five analyzed genes. Putative BPS is underlined. PPT is shown by a bracket. Mutant nucleotides are indicated at E^{+1}. (**B**) RT–PCR of minigenes expressed in HEK293 cells carrying the wild-type (WT) or patient's (PT) nucleotide. The mutations cause exon skipping in *GH1*, *FECH* and *EYA1*, but not in *LPL* and *HEXA*. Mean and SD of three independent experiments of the densitometric ratios of the exon-skipped product is shown at the bottom.

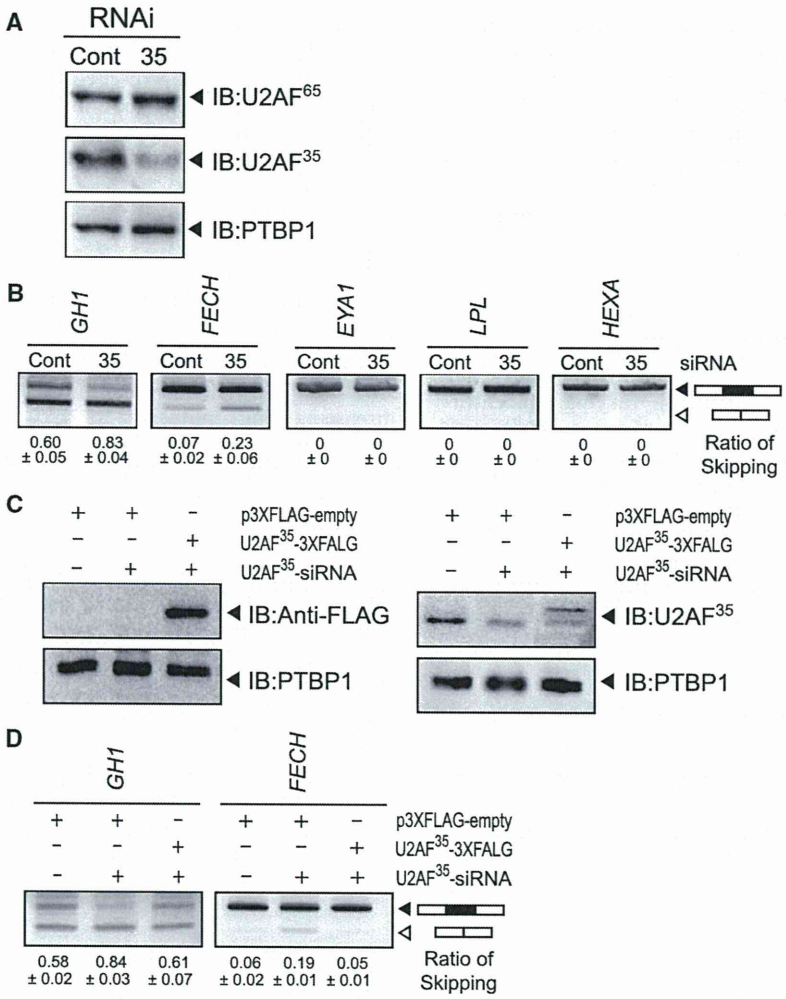

Figure 2. Effects of down-regulation of U2AF^{35} on pre-mRNA splicing. (**A**) Western blots demonstrating that U2AF^{35}-siRNA efficiently knocks down U2AF^{35} but not U2AF^{65} or PTBP1. (**B**) Down-regulation of U2AF^{35} facilitates exon skipping in wild-type *GH1* and *FECH*, but not in wild-type *EYA1*, *LPL* and *HEXA*. (**C**) Introduction of an siRNA-resistant p3XFLAG-U2AF^{35} encoding 3× FLAG fused with U2AF^{35} is visualized by immunoblots against FLAG and U2AF^{35}. (**D**) Exon skipping facilitated by U2AF^{35}-siRNA is partially rescued by introduction of the siRNA-resistant p3XFLAG-U2AF^{35}.

that the U2AF^{35}-siRNA had no effect on the expression level of U2AF^{65}. As expected, the down-regulation of U2AF^{35} increased exon skipping of *GH1* and *FECH* (Figure 2B) but not to the levels of the mutant constructs (Figure 1B). Again, as expected, we observed no effect on *LPL* and *HEXA*. Unexpectedly, however, *EYA1* demonstrated no response to the down-regulation of U2AF^{35}. Less efficient effects of U2AF^{35}-siRNA on *GH1*, *FECH* and *EYA1* (Figure 2B) compared to the mutant constructs (Figure 1B) were likely because the mutation abolished binding of U2AF^{35} in all the cells, whereas substantial numbers of cells failed to incorporate U2AF^{35}-siRNA and gave rise to normally spliced products.

We additionally introduced the siRNA-resistant p3XFLAG-U2AF^{35} to ensure that the effect of siRNA-U2AF^{35} was not due to off-target effects (Figure 2C). As expected, coexpression of p3XFLAG-U2AF^{35} partially rescued the splicing defects in *GH1* and *FECH* (Figure 2D).

U2AF^{35} is required for binding of U2AF^{65} to PPT in *FECH* but not in *LPL*

To further prove that U2AF^{35} is required for pre-mRNA splicing, we employed an electrophoretic mobility shift assay (EMSA) using wild-type and mutant RNA substrates of *FECH* and *LPL* (Figure 3A). His-tagged U2AF^{35} and U2AF^{65} were expressed using bacluovirus and were purified under denatured and native conditions, respectively. Denatured U2AF^{35} was refolded before RNA-EMSA. As expected, U2AF^{65} failed to bind to the wild-type *FECH* in the absence of U2AF^{35}, and addition

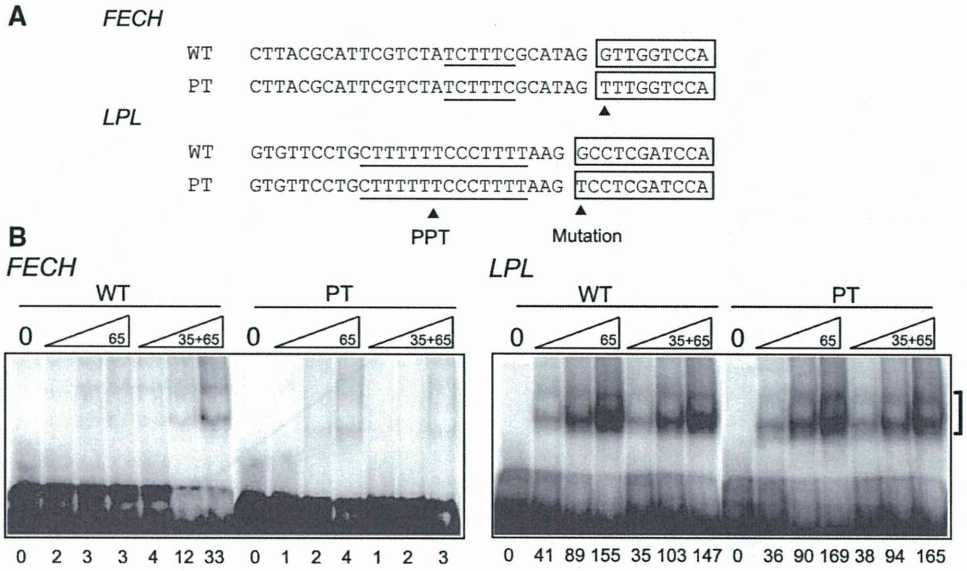

Figure 3. RNA-EMSA. (**A**) Sequences of wild-type (WT) and mutant (PT) RNA probes of *FECH* and *LPL* employed for RNA-EMSA. (**B**) RNA-EMSA of wild-type and mutant *FECH* and *LPL* with increasing amounts of $U2AF^{65}$ with or without $U2AF^{35}$. His-tagged $U2AF^{65}$ and $U2AF^{35}$ are expressed in Sf9 cells and are purified. Wild-type *FECH* requires $U2AF^{35}$ to bind to $U2AF^{65}$, whereas wild-type *LPL* does not require $U2AF^{35}$. A mutation at E^{+1} abrogates binding of $U2AF^{65}$ in *FECH* but not in *LPL*. Concentrations of $U2AF^{35}$ are 5, 10 and 20 ng/μl; and those of $U2AF^{65}$ are 10, 20 and 40 ng/μl. Numbers at the bottom indicate intensities of the retarded fragments in arbitrary units.

of $U2AF^{35}$ gained its binding. For the mutant *FECH*, neither $U2AF^{65}$ alone nor addition of both U2AFs showed binding of U2AFs. On the other hand, the wild-type *LPL* did not require $U2AF^{35}$ to bind to $U2AF^{65}$. Addition of $U2AF^{35}$ did not substantially increased binding of $U2AF^{65}$. These bindings were not affected by the mutation at E^{+1} of *LPL* (Figure 3B).

These results indicate that the mutation in *FECH* compromises a binding affinity for $U2AF^{35}$, which in turn abrogates binding of $U2AF^{65}$ and results in aberrant splicing. On the other hand, wild-type *LPL* does not need to bind to $U2AF^{35}$ and the mutation at E^{+1} has no effect on the assembly of spliceosome.

PPT determines the splicing consequences of the mutations

In an effort to delineate effects of the PPT sequences on the splicing consequence of a mutation at E^{+1}, we introduced a series of mutations into the PPT in the presence of the mutation at E^{+1}. Extensions of the polypyrimidine stretch ameliorated aberrant splicing in *GH1*, *FECH* and *EYA1*. Conversely, truncations or disruptions of the polypyrimidine stretch caused exon skipping in *LPL* and *HEXA* (Figure 4).

Length of the polypyrimidine stretch best predicts the splicing consequences

We next sought for parameters that differentiate normal and aberrant splicings in these minigenes. Analysis of parameters that potentially dictate the strength of the PPT indicated that the length of pyrimidine stretch, the number of pyrimidines in 25 or 50 nt at the 3′-end of an intron correlated with the ratio of exon skipping with correlation coefficients of more than 0.6 (Supplementary Table S1). The number of pyrimidines in 25 or 50 nt at the 3′-end of an intron, however, failed to predict splicing consequences of nine other constructs shown in Figure 6, and is likely to be overfitted parameters unique to the 35 constructs in Figure 4. Coolidge and colleagues report that $(GU)_{11}$ in PPT is partly functional, but we did not observe alternative purine and pyrimidine residues in our PPTs and did not quantify effects of alternative nucleotides (10). We thus took the length of pyrimidine stretch as a best parameter to dictate the strength of the PPT (Figure 5A). The native *GH1*, *FECH* and *EYA1* carry a stretch of 6–10 pyrimidines, whereas the native *LPL* and *HEXA* harbor a stretch of 14 and 13 pyrimidines, respectively (arrows in Figure 5A). For highly degenerate PPTs in the artificial constructs, the total number of pyrimidines in a stretch of 25 nt at the 3′-end of an intron well predicts the ratio of exon skipping (Figure 5B). These analyses revealed that the length of the polypyrimidine stretch should be at least 10–15 nt to ensure normal splicing even in the presence of a mutation at E^{+1}.

Identification of effects on pre-mRNA splicing of nine disease-associated mutations at the first nucleotide of an exon

We next examined other mutations at E^{+1} in which splicing consequences have not been previously analyzed. We first identified 224 mutations that abrogate the first 'G' nucleotide of an exon in the Human Gene Mutation Database at http://www.hgmd.cf.ac.uk/ (data not shown). Among these, we arbitrarily chose nine mutations causing

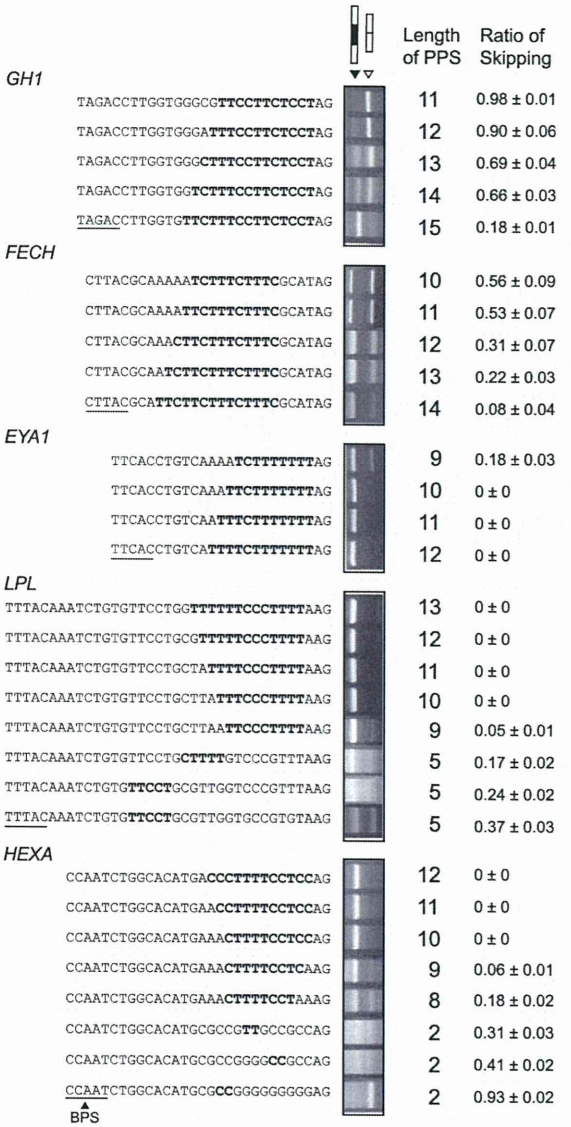

Figure 4. RT–PCR of HEK293 cells transfected with minigenes carrying artificially extended or disrupted PPT's. All the constructs harbor a mutation at E^{+1}. The top construct of each gene represents the patient's sequence. Only the nucleotide sequences of the 3′-end of an intron are indicated. The longest stretches of the polypyrimidines are shown in bold. Underlines indicate putative BPS's. The rightmost column shows the mean and SD of three independent experiments of the densitometric ratios of the exon-skipped product.

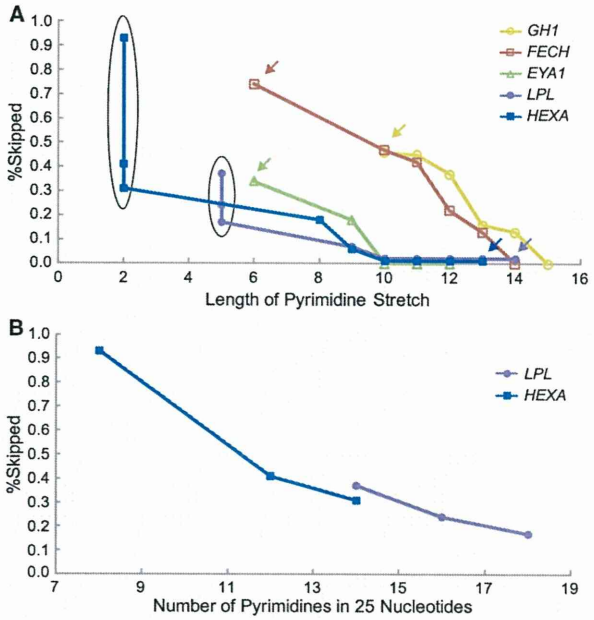

Figure 5. Ratios of exon skipping are plotted against the lengths of the polypyrimidine stretch (**A**) and the numbers of pyrimidines in 25 nt at the 3′-end of an intron (**B**). The ordinate (percent skipped) represents the ratios of exon skipping compared to that of the wild-type construct. The data are obtained from RT–PCR shown in Figure 4. Arrows indicate the original constructs carrying the patient's sequence, and the others are artificial constructs. Six constructs indicated by ovals in (A) are plotted in (B).

neuromuscular and musculoskeletal disorders (Figure 6A).

We constructed nine pairs of wild-type and mutant minigenes, and introduced them into HEK293 cells. We observed aberrant splicing in *PKHD1*, *COL1A2* (exon 37), *CLCN2*, *CAPN3* (exons 10 and 17), but not in *LAMA2*, *NEU1*, *COL6A2* and *COL1A2* (exon 23) (Figure 6B). The lengths of the polypyrimidine stretch of the five aberrantly spliced constructs ranged from 4 to 10 nt, whereas those of the four normally spliced constructs ranged from 9 to 16 nt. These results are in concordance with a notion that the short polypyrimidine stretches are predisposed to aberrant splicing due to a mutation at E^{+1}, whereas long polypyrimidine stretches are tolerant to such mutations. Among the 224 mutations affecting 'G' at E^{+1}, only three mutations have been reported to cause aberrant splicing. We here analyzed nine mutations and identified five more such mutations. It is thus likely that most splicing mutations at E^{+1} still remain unrecognized to date.

Analysis of the 3′-splice sites of the human genome

We next analyzed PPTs of 176 809 introns of the entire human genome. The length of the pyrimidine stretch was shorter when E^{+1} was the conserved 'G' (Figure 7A). This also supports a notion that AG-dependent 3′ ss harboring G at E^{+1} has a short polypyrimidine stretch (12). In addition, the ratio of 'C' at intronic position −3 was lower when E^{+1} was the conserved 'G' (Figure 7B), which suggests that G at E^{+1} makes C at −3 dispensable for binding to $U2AF^{35}$, although this is not directly relevant to the length of the PPT.

Being prompted by a previous report that $U2AF^{35}$ binds up to the 10th nucleotide of an exon (12), we examined nucleotide frequencies at exonic positions +1

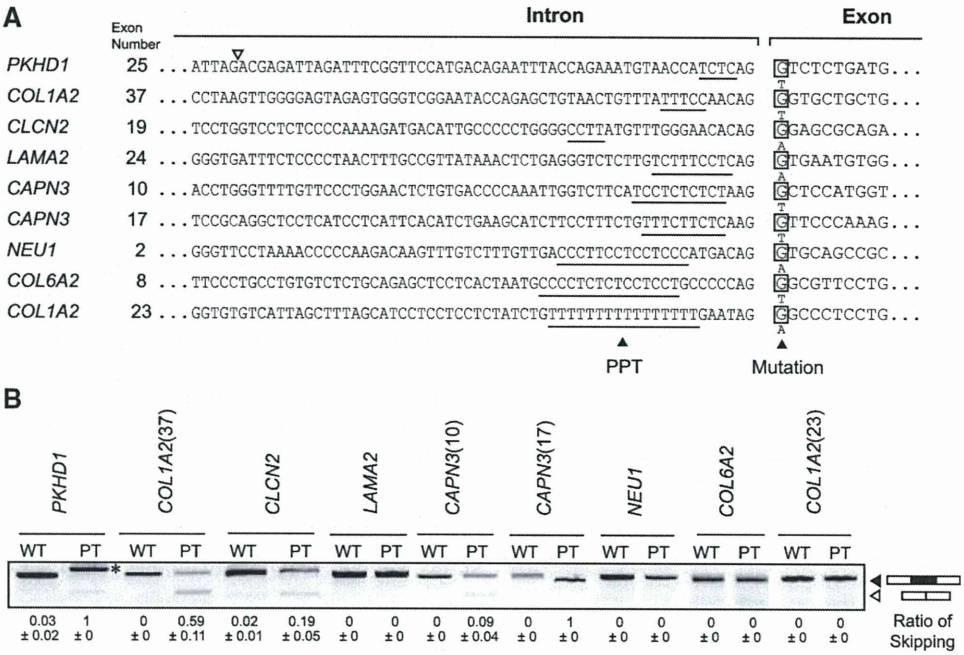

Figure 6. RT–PCR analysis of nine disease-causing mutations at E^{+1}. (**A**) Sequences at the intron/exon junctions of nine pairs of wild-type and mutant constructs. The longest polypyrimidine stretches are underlined. (**B**) RT–PCR of minigenes transfected into HEK293 cells. Five mutant constructs are aberrantly spliced, whereas the remaining four mutants are normally spliced. Numbers in the parentheses indicate exon numbers. In *PKHD1*, a cryptic 3′-splice site (open arrowhead in panel A) at 55 nt upstream of the native site is activated (asterisk). Mean and SD of three independent experiments of the densitometric ratios of the exon-skipped product is shown at the bottom.

to +12. We counted only wobbling nucleotides based on the human genome annotation NCBI Build 37.1 (hg19). As expected, 'GT' dinucleotide was frequently observed at exonic positions +1 and +2. We also observed preference for a 'T' nucleotide at positions +3 to +5 (Figure 7C). Alignment of SELEX results of $U2AF^{35}$ by Wu and colleagues (12) similarly demonstrate overrepresentation of 'T' nucleotides at positions +3 to +6 (Figure 7D). We thus analyzed effects of 'TTT' at positions +3 to +5 using the *GH1, FECH* and *EYA1* minigenes carrying the patient's mutations. We found that introduction of 'TTT' at exonic position +3 to +5 had no effect in *GH1* and *FECH*, but slightly enhanced exon recognition in *EYA1* (Figure 7E).

DISCUSSION

We previously reported that the SD-score algorithm efficiently predicts splicing consequences of a mutation affecting the 5′ ss (32). We next identified that the human BPS consensus is simply yUnAy (5), and hoped to predict if a given mutation affecting the BPS causes aberrant splicing or not. The high degeneracy of the BPS consensus, however, prevented us from constructing an efficient algorithm. In this communication, we worked on mutations at E^{+1}. As far as we know, only three such mutations have been reported to cause aberrant splicing, and only two such mutations have been reported not to affect splicing. Knockdown and RNA-EMSA of $U2AF^{35}$, as well as analyses of artificial PPT mutations and nine disease-causing mutations at E^{+1} revealed that AG-dependence of 3′ ss determines the splicing consequences. In the presence of a mutation at E^{+1}, a stretch of 15 or more pyrimidines ensures normal splicing, whereas a stretch of 10 or less pyrimidines are predisposed to aberrant splicing.

AG-dependent 3′ ss requires both $U2AF^{65}$ and $U2AF^{35}$ to bring U2snRNP to the branch point, whereas AG-independent 3′ ss has a long stretch of pyrimidines that can bind to $U2AF^{65}$ without $U2AF^{35}$ (13,15). $U2AF^{35}$ potentially provides an additional RNA–protein interacting force and an additional SR protein-binding surfaces (33). An artificial G-to-C mutation at E^{+1} downstream of a stretch of five pyrimidines in the mouse IgM gene abrogates binding of $U2AF^{35}$ and causes defective splicing (14). Similarly, in *INSR* exon 11 carrying an 'A' nucleotide at E^{+1}, a stretch of 14 pyrimidines but not of 10 pyrimidines is properly spliced (34). Additionally, a stretch of eight pyrimidines upstream of the last exon with 'C' at E^{+1} of *EIF3S7* is dependent on $U2AF^{35}$, whereas a stretch of 14 pyrimidines upstream of the last exon with 'A' at E^{+1} of *CUEDC1* is independent (15). Our observations and previous reports all point to a notion that effects on pre-mRNA splicing should be scrutinized for a mutation at E^{+1} if the preceding intron carries a short stretch of 10 or less pyrimidines. Indeed, in our analysis of nine disease-causing mutations, five of six mutants with 10 or less contiguous pyrimidines were aberrantly spliced (Figure 6), but no splicing analysis has been documented for any of them.

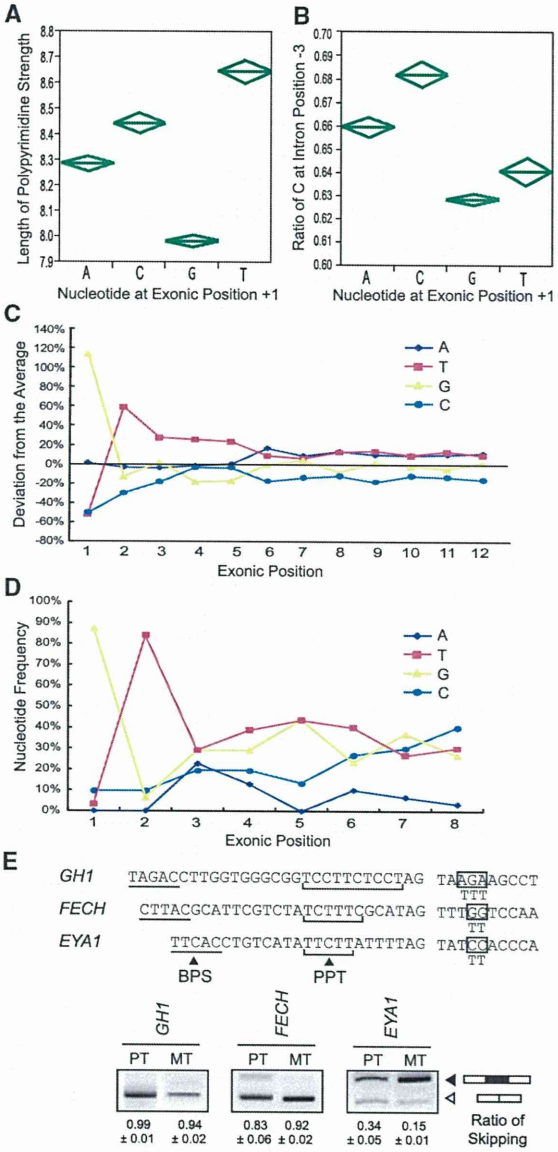

Figure 7. (**A**) Polypyrimidine stretch and the first nucleotide of an exon in the human genome. The longest stretch of uninterrupted pyrimidines among 25 nt at the 3′-ends of an intron is counted for 176 809 introns of the human genome. Diamonds represent means and 95% confidence intervals. One-way ANOVA and Fisher's-multiple range test revealed statistical significance of $P < 0.0001$. (**B**) Ratios of 'C' at position −3 in relation to the first nucleotide of an exon are analyzed for 176 809 introns of the human genome. Diamonds represent means and 95% confidence intervals. One-way ANOVA and Fisher's-multiple range test revealed statistical significance of $P < 0.0001$. (**C**) Preferentially observed nucleotides at the 5′-end of an exon in human. Only wobbling nucleotides are counted in the human genome. (**D**) Nucleotide frequencies at exonic positions +1 to +8 according to the SELEX data of U2AF^{35} by Wu and colleagues (12). (**E**) Effects of 'TTT' at exonic positions +3 to +5 in *GH1*, *FECH* and *EYA1* carrying the patient's mutation at E^{+1}. Artificially substituted exonic nucleotides are indicated by boxes. Mean and SD of three independent experiments of the densitometric ratios of the exon-skipped product is shown at the bottom.

We first report overrepresentation of 'T' nucleotides at exonic positions +3 to +5 in the human genome, as well as in *in vitro* U2AF^{35}-binding sites. Enhancement of exon recognition in *EYA1* by introduction of 'TTT' at positions +3 to +5 also underscores a notion that 'TTT' at +3 to +5 is likely to enhance binding of U2AF^{35}. Effects of 'TTT', however, were not observed in *GH1* and *FECH*. As the patient's mutation in *GH1* and *FECH* resulted in almost complete skipping of an exon, whereas that in *EYA1* gave rise to both exon-skipped and included products. The degrees of aberration of exon recognition may account for the 'TTT'-responsiveness. Alternatively, although no ESE motif was detected in the 'TTT'-introduced *EYA1* by five different ESE search tools, an unrecognized ESE might have ameliorated exon skipping in *EYA1*. Further analysis is required to elucidate effects of overrepresentation of 'T' at positions +3 to +5.

SUPPLEMENTARY DATA

Supplementary Data are available at NAR Online.

FUNDING

Grants-in-Aids from the Ministry of Education, Culture, Sports, Science and Technology of Japan; Ministry of Health, Labor and Welfare of Japan. Funding for open access charge: Innovative Cell Biology by Innovative Technology granted by the Japan Science and Technology Agency (JST).

Conflict of interest statement. None declared.

REFERENCES

1. Black,D.L. (2003) Mechanisms of alternative pre-messenger RNA splicing. *Annu. Rev. Biochem.*, **72**, 291–336.
2. Jurica,M.S. and Moore,M.J. (2003) Pre-mRNA splicing: awash in a sea of proteins. *Mol. Cell*, **12**, 5–14.
3. Reed,R. (1996) Initial splice-site recognition and pairing during pre-mRNA splicing. *Curr. Opin. Gen. Dev.*, **6**, 215–220.
4. Parker,R., Siliciano,P.G. and Guthrie,C. (1987) Recognition of the TACTAAC box during mRNA splicing in yeast involves base pairing to the U2-like snRNA. *Cell*, **49**, 229–239.
5. Gao,K., Masuda,A., Matsuura,T. and Ohno,K. (2008) Human branch point consensus sequence is yUnAy. *Nucleic Acids Res.*, **36**, 2257–2267.
6. Zorio,D.A. and Blumenthal,T. (1999) Both subunits of U2AF recognize the 3′ splice site in Caenorhabditis elegans. *Nature*, **402**, 835–838.
7. Merendino,L., Guth,S., Bilbao,D., Martinez,C. and Valcarcel,J. (1999) Inhibition of msl-2 splicing by Sex-lethal reveals interaction between U2AF35 and the 3′ splice site AG. *Nature*, **402**, 838–841.
8. Kielkopf,C.L., Rodionova,N.A., Green,M.R. and Burley,S.K. (2001) A novel peptide recognition mode revealed by the X-ray structure of a core U2AF35/U2AF65 heterodimer. *Cell*, **106**, 595–605.
9. Mullen,M.P., Smith,C.W., Patton,J.G. and Nadal-Ginard,B. (1991) Alpha-tropomyosin mutually exclusive exon selection: competition between branchpoint/polypyrimidine tracts determines default exon choice. *Genes Dev.*, **5**, 642–655.
10. Coolidge,C.J., Seely,R.J. and Patton,J.G. (1997) Functional analysis of the polypyrimidine tract in pre-mRNA splicing. *Nucleic Acids Res.*, **25**, 888–896.

11. Soares,L.M., Zanier,K., Mackereth,C., Sattler,M. and Valcarcel,J. (2006) Intron removal requires proofreading of U2AF/3′ splice site recognition by DEK. *Science*, **312**, 1961–1965.
12. Wu,S., Romfo,C.M., Nilsen,T.W. and Green,M.R. (1999) Functional recognition of the 3′ splice site AG by the splicing factor U2AF35. *Nature*, **402**, 832–835.
13. Guth,S., Martinez,C., Gaur,R.K. and Valcarcel,J. (1999) Evidence for substrate-specific requirement of the splicing factor U2AF(35) and for its function after polypyrimidine tract recognition by U2AF(65). *Mol. Cell. Biol.*, **19**, 8263–8271.
14. Guth,S., Tange,T.O., Kellenberger,E. and Valcarcel,J. (2001) Dual function for U2AF(35) in AG-dependent pre-mRNA splicing. *Mol. Cell. Biol.*, **21**, 7673–7681.
15. Pacheco,T.R., Coelho,M.B., Desterro,J.M., Mollet,I. and Carmo-Fonseca,M. (2006) In vivo requirement of the small subunit of U2AF for recognition of a weak 3′ splice site. *Mol. Cell. Biol.*, **26**, 8183–8190.
16. Vorechovsky,I. (2006) Aberrant 3′ splice sites in human disease genes: mutation pattern, nucleotide structure and comparison of computational tools that predict their utilization. *Nucleic Acids Res.*, **34**, 4630–4641.
17. Lefevre,S.H., Chauveinc,L., Stoppa-Lyonnet,D., Michon,J., Lumbroso,L., Berthet,P., Frappaz,D., Dutrillaux,B., Chevillard,S. and Malfoy,B. (2002) A T to C mutation in the polypyrimidine tract of the exon 9 splicing site of the RB1 gene responsible for low penetrance hereditary retinoblastoma. *J. Med. Genet.*, **39**, E21.
18. Faustino,N.A. and Cooper,T.A. (2003) Pre-mRNA splicing and human disease. *Genes Dev.*, **17**, 419–437.
19. Wang,X.-H., Poh-Fitzpatrick,M., Chen,T., Malavade,K., Carriero,D. and Piomelli,S. (1995) Systematic screening for RNA with skipped exons - splicing mutations of the ferrochelatase gene. *Biochim. Biophys. Acta*, **1271**, 358–362.
20. Takahashi,I., Takahashi,T., Komatsu,M., Sato,T. and Takada,G. (2002) An exonic mutation of the GH-1 gene causing familial isolated growth hormone deficiency type II. *Clin. Genet.*, **61**, 222–225.
21. Okada,K., Inoue,A., Okada,M., Murata,Y., Kakuta,S., Jigami,T., Kubo,S., Shiraishi,H., Eguchi,K., Motomura,M. *et al.* (2006) The muscle protein Dok-7 is essential for neuromuscular synaptogenesis. *Science*, **312**, 1802–1805.
22. Ikeda,Y., Takagi,A., Nakata,Y., Sera,Y., Hyoudou,S., Hamamoto,K., Nishi,Y. and Yamamoto,A. (2001) Novel compound heterozygous mutations for lipoprotein lipase deficiency. A G-to-T transversion at the first position of exon 5 causing G154V missense mutation and a 5′ splice site mutation of intron 8. *J. Lipid Res.*, **42**, 1072–1081.
23. Petroulakis,E., Cao,Z., Clarke,J.T., Mahuran,D.J., Lee,G. and Triggs-Raine,B. (1998) W474C amino acid substitution affects early processing of the alpha-subunit of beta-hexosaminidase A and is associated with subacute G(M2) gangliosidosis. *Hum. Mutat.*, **11**, 432–442.
24. Kralovicova,J. and Vorechovsky,I. (2010) Allele-specific recognition of the 3′ splice site of INS intron 1. *Hum. Genet.*, **128**, 383–400.
25. Cartegni,L., Wang,J., Zhu,Z., Zhang,M.Q. and Krainer,A.R. (2003) ESEfinder: a web resource to identify exonic splicing enhancers. *Nucleic Acids Res.*, **31**, 3568–3571.
26. Smith,P.J., Zhang,C., Wang,J., Chew,S.L., Zhang,M.Q. and Krainer,A.R. (2006) An increased specificity score matrix for the prediction of SF2/ASF-specific exonic splicing enhancers. *Hum. Mol. Genet.*, **15**, 2490–2508.
27. Fairbrother,W.G., Yeh,R.F., Sharp,P.A. and Burge,C.B. (2002) Predictive identification of exonic splicing enhancers in human genes. *Science*, **297**, 1007–1013.
28. Wang,Z., Rolish,M.E., Yeo,G., Tung,V., Mawson,M. and Burge,C.B. (2004) Systematic identification and analysis of exonic splicing silencers. *Cell*, **119**, 831–845.
29. Zhang,X.H. and Chasin,L.A. (2004) Computational definition of sequence motifs governing constitutive exon splicing. *Genes Dev.*, **18**, 1241–1250.
30. Zhang,X.H., Kangsamaksin,T., Chao,M.S., Banerjee,J.K. and Chasin,L.A. (2005) Exon inclusion is dependent on predictable exonic splicing enhancers. *Mol. Cell. Biol.*, **25**, 7323–7332.
31. Goren,A., Ram,O., Amit,M., Keren,H., Lev-Maor,G., Vig,I., Pupko,T. and Ast,G. (2006) Comparative analysis identifies exonic splicing regulatory sequences–the complex definition of enhancers and silencers. *Mol. Cell*, **22**, 769–781.
32. Sahashi,K., Masuda,A., Matsuura,T., Shinmi,J., Zhang,Z., Takeshima,Y., Matsuo,M., Sobue,G. and Ohno,K. (2007) In vitro and in silico analysis reveals an efficient algorithm to predict the splicing consequences of mutations at the 5′ splice sites. *Nucleic Acids Res.*, **35**, 5995–6003.
33. Graveley,B.R. (2001) Alternative splicing: increasing diversity in the proteomic world. *Trends Genet.*, **17**, 100–107.
34. Kosaki,A., Nelson,J. and Webster,N.J. (1998) Identification of intron and exon sequences involved in alternative splicing of insulin receptor pre-mRNA. *J. Biol. Chem.*, **273**, 10331–10337.

Biochemical and Biophysical Research Communications 411 (2011) 143–149

Contents lists available at ScienceDirect

Biochemical and Biophysical Research Communications

journal homepage: www.elsevier.com/locate/ybbrc

Molecular hydrogen inhibits lipopolysaccharide/interferon γ-induced nitric oxide production through modulation of signal transduction in macrophages

Tomohiro Itoh [a,b], Nanako Hamada [a], Riyako Terazawa [a], Mikako Ito [c], Kinji Ohno [c], Masatoshi Ichihara [d], Yoshinori Nozawa [a,e], Masafumi Ito [a,*]

[a] Department of Longevity and Aging Research, Gifu International Institute of Biotechnology, 1-1 Naka-fudogaoka, Kakamigahara, Gifu 504-0838, Japan
[b] Faculty of Agriculture, Kinki University, 3327-204 Nakamachi, Nara 631-8505, Japan
[c] Division of Neurogenetics, Center for Neurological Diseases and Cancer, Nagoya University Graduate School of Medicine, 65 Tsurumai, Showa-ku, Nagoya, Aichi 466-8550, Japan
[d] Department of Biomedical Sciences, College of Life and Health Sciences, Chubu University, 1200 Matsumoto-cho, Kasugai, Aichi 487-8501, Japan
[e] Department of Food and Health, Tokai Gakuin University, 5-68 Naka-kirinocho, Kakamigahara, Gifu 504-8511, Japan

ARTICLE INFO

Article history:
Received 7 June 2011
Available online 23 June 2011

Keywords:
Molecular hydrogen
Lipopolysaccharide/interferon γ
Macrophage
Signal transduction
Inflammatory arthritis

ABSTRACT

Molecular hydrogen has been reported to be effective for a variety of disorders and its effects have been ascribed to the reduction of oxidative stress. However, we have recently demonstrated that hydrogen inhibits type I allergy through modulating intracellular signal transduction. In the present study, we examined the hydrogen effects on lipopolysaccharide/interferon γ LPS/IFNγ-induced nitric oxide (NO) production in murine macrophage RAW264 cells. Treatment with hydrogen reduced LPS/IFNγ-induced NO release, which was associated with a diminished induction of inducible isoform of nitric oxide synthase (iNOS). Hydrogen treatment inhibited LPS/IFNγ-induced phosphorylation of apoptosis signal-regulating kinase 1 (ASK1) and its downstream signaling molecules, p38 MAP kinase and JNK, as well as IκBα, but did not affect activation of NADPH oxidase and production of reactive oxygen species (ROS). As ROS is an upstream activator of ASK1, inhibition of ASK1 by hydrogen without suppressing ROS implies that a potential target molecule of hydrogen should be located at the receptor or immediately downstream of it. These results suggested a role for molecular hydrogen as a signal modulator. Finally, oral intake of hydrogen-rich water alleviated anti-type II collagen antibody-induced arthritis in mice, a model for human rheumatoid arthritis. Taken together, our studies indicate that hydrogen inhibits LPS/IFNγ-induced NO production through modulation of signal transduction in macrophages and ameliorates inflammatory arthritis in mice, providing the molecular basis for hydrogen effects on inflammation and a functional interaction between two gaseous signaling molecules, NO and molecular hydrogen.

1. Introduction

Accumulating evidence suggest that molecular hydrogen is effective for a number of disorders including oxidative stress-related diseases and inflammatory diseases [1]. In animal disease models, inhalation of hydrogen gas protects against cerebral infarction [2], myocardial infarction, hepatic ischemia, neonatal hypoxic brain injury, small intestine and lung transplantation, zymosan-induced inflammation, inflammatory bowel disease and sepsis. Oral intake of hydrogen-rich water exerts beneficial effects on stress-induced learning impairment, atherosclerosis, Parkinson's disease, kidney transplantation and hearing disturbance. Infusion of hydrogen-rich saline also alleviates acute pancreatitis, spinal cord injury and obstructive jaundice. In humans, oral intake of hydrogen-rich water improves lipid and glucose metabolism in patients with diabetes and impaired glucose tolerance. In most of studies, hydrogen effects have been ascribed to the reduction of oxidative stress.

We have recently demonstrated a preventive effect of oral intake of hydrogen-rich water on type I allergy in a mouse model, which is not causally associated with oxidative stress [3]. In cultured mast cells, we investigated the underlying mechanisms and found that hydrogen attenuates degranulation by inhibiting the high affinity IgE receptor (FcεRI)-mediated signal transduction but not by reducing oxidative stress. Based on these observations, we proposed that modulation of signaling pathways may be an essential mechanism underlying hydrogen effects on a broad spectrum of diseases and that hydrogen may be a gaseous signaling molecule like nitric oxide (NO).

NO is involved in a variety of important physiological processes such as vasodilatation, neurotransmission and host defense against

* Corresponding author. Fax: +81 58 371 4412.
E-mail address: mito@giib.or.jp (M. Ito).

0006-291X/$ - see front matter © 2011 Elsevier Inc. All rights reserved.
doi:10.1016/j.bbrc.2011.06.116

invading pathogens [4]. However, an excessive amount of NO is detrimental, resulting in rheumatoid arthritis, gastritis, bowel inflammation and bronchitis [5,6]. In macrophages, NO is synthesized by inducible isoform of nitric oxide synthase (iNOS), which catalyzes the reaction of L-arginine to L-citrulline and NO, in response to various stimuli such as lipopolysaccharide (LPS), interferon (IFN), tumor necrosis factor α (TNFα) and interleukin 1β (IL1β) [7]. LPS binds to the cell surface receptor CD14, which triggers activation of toll like receptor 4 (TLR4) and the downstream signaling molecules such as IκB and mitogen-activated protein kinases (MAPKs) including c-Jun NH_2-terminal protein kinase (JNK), p38 MAP kinase and extracellular signal-regulated kinase (ERK) [8]. TLR4 signaling activates transcription factors such as nuclear factor kappa B (NFκB), activator protein 1 (AP1) and ELK1, culminating in the expression of pro-inflammatory genes including iNOS, cyclooxygenase 2 (COX2), TNFα and IFNβ. On the other hand, IFNβ and INFγ, respectively, bind to type I and type II IFN receptors expressed on the surface of macrophages, and activate Janus kinase (JAK)–signal transducers and activators of transcription (STAT) signaling, resulting in up-regulation of IFN regulatory factor 1 (IRF1) [9]. Both IRF1 and STAT1 bind to the iNOS promoter and enhance production of NO.

Previous reports have demonstrated that hydrogen treatment attenuates inflammation in animal models of inflammatory diseases such as zymosan-induced inflammation [10] and inflammatory bowel disease [11], but the underlying molecular mechanisms are not yet understood. According to our recent findings [3], we hypothesized that hydrogen might modulate the inflammatory signal transduction and that there might be a functional interaction between two gaseous signaling molecules, NO and molecular hydrogen. In the present study, we examined the effects of hydrogen on LPS/IFNγ-induced signal transduction and NO production in murine RAW264 macrophage cells. We also studied the hydrogen effects on anti-type II collagen antibody-induced arthritis in mice, a model for human rheumatoid arthritis.

2. Materials and methods

2.1. Antibodies

The antibodies to p-ASK1 (Ser967/Thr845), AKT, p-AKT, p44/42 MAP kinase (ERK1/2), p-p44/42 MAP kinase (Thr202/204), SAPK/JNK, p-SAPK/JNK (Thr180/Tyr204), p38 MAP kinase, p-p38 MAP kinase (Thr180/Tyr182), iNOS, COX2 TAK1, p-TAK1 (Ser412/Thr184/187), IκBα, p-IκBα (Ser32/36), NFκB p65, STAT1α and p-STAT1α (Tyr701) were purchased from Cell Signaling Technology (Beverly, CA, USA). The antibodies against $p22^{phox}$, $p47^{phox}$, $p67^{phox}$ and $gp91^{phox}$ were from Santa Cruz Biotechnology (Santa Cruz, CA, USA). Anti-ASK1, -histone H3 and -β-actin antibodies were obtained from Abcam (Cambridge, MA, USA), Upstate (Lake Placid, NY, USA) and Sigma–Aldrich (St. Louis, MO, USA), respectively.

2.2. Cell culture and hydrogen treatment

Murine macrophage RAW264 cells were purchased from RIKEN BioResource Center (Tsukuba, Japan) and cultured in Dulbecco's modified Eagle's medium (DMEM) containing 10% heat-inactivated fetal bovine serum (FBS), 100 U/ml of penicillin and 100 μg/ml streptomycin in a humidified atmosphere of 5% CO_2 at 37 °C. Hydrogen treatment was performed as described previously with a slight modification [3]. Briefly, cells seeded onto multi-well plates were incubated at 37 °C under a humidified condition of 75% H_2, 20% O_2 and 5% CO_2, or 95% air and 5% CO_2 in a small aluminum bag. After 24 h incubation in the presence of hydrogen, the hydrogen concentration in the culture media was about 0.3 ppm as measured by using the H_2–N hydrogen needle sensor (Unisense, Aarhus, Denmark). After treatment with or without hydrogen for 24 h, cells were treated with or without LPS (final concentration, 200 ng/ml) (Sigma–Aldrich) and IFNγ (final concentration, 25 ng/ml) (Millipore, Bedford, MA, USA), which was followed by incubation in the presence or absence of hydrogen.

2.3. Measurement of nitric oxide production

Cell culture media were centrifuged at 4 °C for 5 min and the supernatant was subjected to measurement of the amount of nitrite, a stable metabolite of NO, using the Griess reagent kit (Promega, Madison, WI, USA).

2.4. Western blot analysis

Whole cell extracts were prepared by lysing in RIPA buffer containing the complete protease inhibitor cocktail and the phosphatase inhibitor cocktail (Roche, Penzberg, Germany). The cytosolic and nuclear fractions were separated by the NE-PER nuclear and cytoplasmic extraction kit (Thermo Fisher Scientific, Waltham, MA, USA). The cytosolic and membrane fractions were isolated using the ProteoExtract subcellular proteome extraction kit (Merk KGaA, Darmstdt, Germany). Samples were subjected to sodium dodecyl sulfate–polyacrylamide gel electrophoresis (SDS–PAGE) and electroblotted onto PVDF membranes. Membranes were incubated with a primary antibody, followed by incubation with a horseradish peroxidase-conjugated secondary antibody. Immunolabeled proteins were detected using the ECL chemiluminescence kit (GE Healthcare, Piscataway, NJ, USA) and the LAS-4000 lumino-image analyzer (Fujifilm, Tokyo, Japan).

2.5. Quantitative RT-PCR

Total RNA was extracted from cells by the TRIzol reagent (Invitrogen, Carlsbad, CA, USA) followed by DNase I treatment. cDNA was synthesized using the PrimeScript reagent kit (Takara Bio, Ohtsu, Japan) and subjected to quantitative RT-PCR using the Thermal Cycler Dice real-time PCR system (TP800, Takara Bio). Primers for *iNOS* and *GAPDH* were purchased from Takara Bio. The expression level of *iNOS* gene was determined using the comparative C_t method and normalized to that of *GAPDH*. The PCR consisted of 45 cycles (95 °C for 10 s, 60 °C for 40 s and 72 °C for 1 s) after an initial denaturation step (95 °C for 10 min).

2.6. Measurement of intracellular ROS levels

Intracellular levels of reactive oxygen species (ROS) were determined using a cell-permeable fluorescent probe, CM-H_2DCF-DA (Invitrogen). Cells were incubated with 10 μM CM-H_2DCF-DA for 1 h at 37 °C. After treatment, cells were washed twice with PBS and lysed in RIPA buffer. The absorbance of the lysates was measured with excitation at 490 nm and emission at 530 nm using the MTP-600 fluorometric imaging plate reader (Corona Electric, Ibaraki, Japan).

2.7. Hydrogen treatment of mice

Five-weeks-old female BALB/c Cr Slc mice (Japan SLC, Hamamatsu, Japan) were fed with either hydrogen-rich or control water *ad libitum*, as described previously [3]. Hydrogen-rich water packed in aluminum pouches was purchased from Blue Mercury (Tokyo, Japan). The hydrogen concentration of the hydrogen-rich water was approximately 1.0 ppm. The control water was prepared by gently stirring the hydrogen-rich water in open air for 24 h. This study was approved by the Animal Use Committee of the Gifu

International Institute of Biotechnology and the animals were maintained according to the guidelines for the care of laboratory animals of the Gifu International Institute of Biotechnology.

2.8. Anti-type II collagen antibody-induced arthritis in mice

Inflammatory arthritis was induced using the arthritogenic mouse monoclonal anti-type II collagen 5 clone antibody cocktail (Iwai Chemical, Tokyo, Japan). Seven-weeks-old mice, which were fed with either hydrogen-rich or control water for 2 weeks, were injected intravenously with 1 mg of the arthritogenic cocktail. Hydrogen treatment continued after the injection. Three days later, 25 μg of LPS (*Escherichia coli* O111:B4) was injected intraperitoneally. Two weeks after the antibody injection, we took photographs of the hind and front paws, evaluated the arthritis scores and measured the foot volume of hind paws using the plethysmometer (MK550M, Muromachi-kikai, Tokyo, Japan). The arthritis score was determined by grading each of four paws on a 0–4 scale [12]. Thus, the total arthritis score of a given mouse varies in the range 0–16.

2.9. Statistical analysis

All data were analyzed using Student's *t*-test or two-way ANOVA followed by Fisher's multiple range test.

3. Results

3.1. Hydrogen inhibits LPS/IFNγ-induced NO release from RAW264 macrophage cells

Hydrogen treatment for 24 h did not affect cell viability and proliferation (data not shown). In order to explore possible interaction between NO and hydrogen, we examined the effects of hydrogen on LPS/IFNγ-induced NO release from murine RAW264 macrophage cells. Treatment with hydrogen significantly reduced the NO levels in the culture media, the inhibitory effect being more pronounced at 12 h than at 6 h after LPS/IFNγ stimulation (Fig. 1A). These results suggest that there exists a functional relationship between NO and hydrogen.

3.2. Hydrogen inhibits LPS/IFNγ-induced iNOS expression

Stimulation with LPS/IFNγ up-regulates expression of pro-inflammatory genes such as iNOS and COX2. As shown in Fig. 1B, LPS/IFNγ stimulation resulted in a robust increase in protein expression of iNOS and COX2 at 6 h after treatment, which was markedly suppressed by treatment with hydrogen. Consistent with these findings, quantitative RT-PCR demonstrated that hydrogen inhibits LPS/IFNγ-induced mRNA expression of *iNOS* at 3 h after stimulation (Fig. 1C). These results indicate that hydrogen is capable of inhibiting LPS/IFNγ-induced expression of iNOS, which may account for suppression by hydrogen of LPS/IFNγ-induced NO release from macrophage cells (Fig. 1A).

3.3. Hydrogen inhibits LPS/IFNγ-mediated signal transduction

LPS signaling enhances phosphorylation of MAPKs and IκBα, and thereby activates transcription factors such as AP1, ELK1 and NFκB, whereas IFNγ signaling increases expression of IRF1 via activation of JAK–STAT signaling. These transcription factors activated or up-regulated by LPS/IFNγ stimulation bind to the iNOS promoter and enhance NO production. LPS/IFNγ stimulation enhanced phosphorylation of MAPKs including p38, JNK and ERK as well as AKT and STAT1α (Fig. 2A). Hydrogen treatment inhibited LPS/IFNγ-induced phosphorylation of p38 and JNK, but did not affect that of ERK, AKT and STAT1α.

Phosphorylation of IκB proteins leads to its degradation and NFκB translocation into the nucleus. As shown in Fig. 2B, LPS/IFNγ stimulation enhanced phosphorylation of IκBα and reduced its cytosolic level, which was associated with a decrease in NFκB p65 subunit in the cytosol and its increase in the nuclei. Treatment with hydrogen suppressed the LPS/IFNγ-induced activation of the NFκB pathway.

Taken together, these results suggest that hydrogen suppresses LPS/IFNγ-mediated signal transduction by inhibiting phosphorylation of p38, JNK and IκBα, resulting in reduced iNOS expression and NO production.

3.4. Hydrogen inhibits LPS/IFNγ-induced phosphorylation of ASK1

Among protein kinases activated by LPS/IFNγ, p38, JNK and IκBα were specifically inhibited by hydrogen (Fig. 2A and B). Apoptosis signal-regulating kinase 1 (ASK1), which is activated by endotoxins such as LPS, has been shown to activate both p38 and JNK MAPKs [13]. We thus investigated whether ASK1 phosphorylation is affected by hydrogen. As shown in Fig. 2C, phosphorylation of ASK1 at Ser967 and Thr845 caused by LPS/IFNγ stimulation was attenuated by hydrogen treatment. In contrast, LPS/IFNγ-induced phosphorylation of TGFβ-activated kinase 1 (TAK1) at Ser412 and Thr184/187, which, as well as ASK1, has been implicated in TNF receptor associated factor (TRAF)-dependent signaling pathways [14], was not affected by treatment with hydrogen. These results indicate that hydrogen inhibits LPS/IFNγ-induced phosphorylation of ASK1.

3.5. Hydrogen does not affect LPS/IFNγ-induced NOX activation and ROS production

It has been shown that ASK1 is activated by endotoxins such as LPS through ROS production, which in turn activates p38 and JNK MAPKs [15]. Furthermore, a direct link between ASK1 and NADPH oxidase (NOX) has been reported [16]. Here we investigated whether inhibition by hydrogen of LPS/IFNγ-induced ASK activation is mediated by suppression of NOX activation and ROS production. As shown in Fig. 3A, hydrogen treatment did not affect LPS/IFNγ-induced ROS production. For NOX activation, in response to LPS/IFNγ stimulation, the levels of the cytosolic subunits of NOX, $p47^{phox}$ and $p67^{phox}$, were decreased in the cytosolic fraction and increased in the membrane fraction (Fig. 3B). However, treatment with hydrogen did not influence the LPS/IFNγ-induced translocation of $p47^{phox}$ and $p67^{phox}$ to the membranes. These results suggest that hydrogen does not affect LPS/IFNγ-induced NOX activation and ROS production.

3.6. Oral intake of hydrogen-rich water ameliorates anti-type II collagen antibody-induced arthritis in mice

The findings that hydrogen suppressed LPS/IFNγ-induced NO production in cultured macrophage cells prompted us to examine whether oral intake of hydrogen-rich water could ameliorate anti-type II collagen antibody-induced arthritis in mice, a model for human rheumatoid arthritis [17]. In this mouse disease model, following the injection of anti-type II collagen-specific monoclonal antibody, LPS is injected to increase the incidence and severity of the disease. As shown in Fig. 4A, erythema and swelling of the hind and front paws were alleviated in mice treated with hydrogen-rich water compared with those treated with control water. The arthritis score was significantly lower in hydrogen-rich water-treated mice than in control water-treated mice (Fig. 4B). Both left and right hind paw volumes were decreased in hydrogen-treated mice

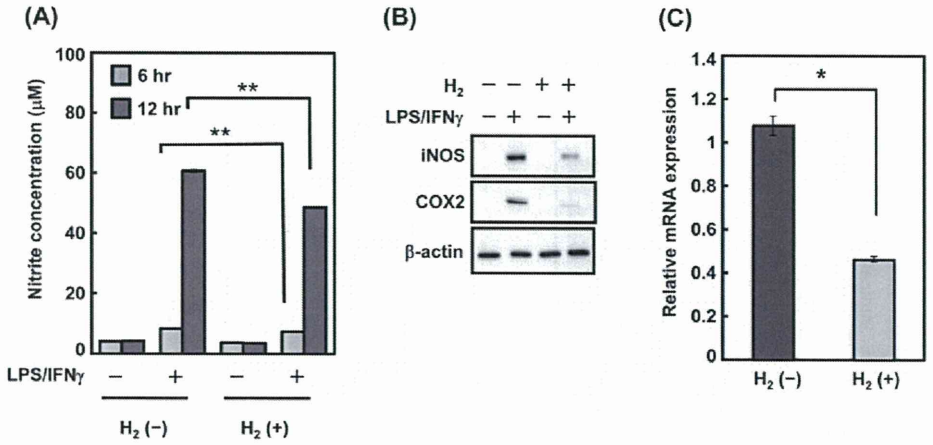

Fig. 1. Effects of hydrogen treatment on LPS/IFNγ-induced NO release and iNOS expression in RAW264 cells. RAW264 cells were incubated for 24 h in the presence or absence of hydrogen and then treated with or without LPS and IFNγ. (A) After incubation in the presence or absence of hydrogen for additional 6 and 12 h, cell culture media were harvested for measurement of nitrite, a stable metabolite of NO (mean ± SD, $n = 9$). Asterisks indicate statistical significance as determined by Student's t-test (**$p < 0.01$). (B) After incubation in the presence or absence of hydrogen for additional 6 h, cell lysates were harvested and subjected to Western blot analysis for iNOS, COX2 and β-actin. A representative blot from three independent experiments is shown. (C) After incubation in the presence or absence of hydrogen for additional 3 h, total RNA was harvested and subjected to quantitative RT-PCR for *iNOS* (mean ± SD, $n = 3$). Asterisks indicate statistical significance as determined by Student's t-test (*$p < 0.05$).

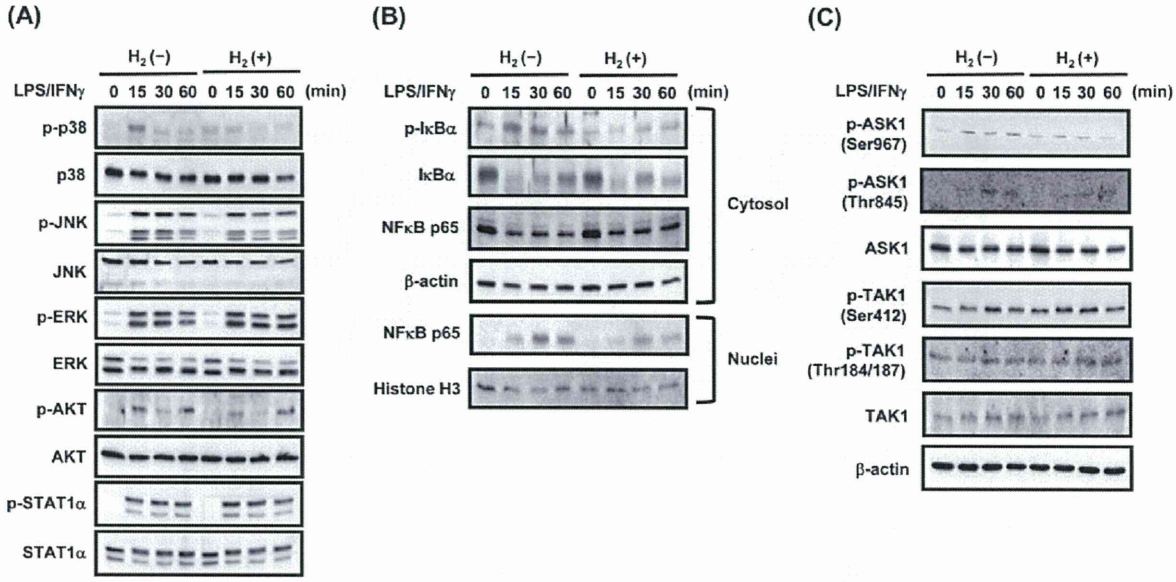

Fig. 2. Effects of hydrogen on LPS/IFNγ-mediated signal transduction in RAW264 macrophage cells. RAW264 macrophage cells were incubated for 24 h in the presence or absence of hydrogen and then treated with or without LPS and IFNγ. After incubation in the presence or absence of hydrogen for indicated time periods, cell lysates (A) and (C) and the cytosolic and nuclear fractions (B) were harvested and subjected to Western blot analysis for indicated proteins. A representative blot from three independent experiments is shown.

compared with control mice, but the statistical significance was observed only for the left hind paw ($p < 0.05$) (Fig. 4C). These results suggest that oral intake of hydrogen-rich water suppresses inflammation and alleviates arthritis in mice.

4. Discussion

Numerous papers have been published showing the efficacy of hydrogen treatment [1] since the first report in 2007 [2], in which specific scavenging of hydroxyl radical has been proposed as a mechanism accounting for the hydrogen effect. Most studies demonstrate reduced oxidative stress by hydrogen and assume that this is a major mechanism underlying the hydrogen effects. However, in type I allergy, hydrogen suppresses phosphorylation of FcεRI-associated Lyn and its downstream signaling molecules, which subsequently inhibits the NOX activity and reduces the generation of hydrogen peroxide [3]. Thus, we concluded that reduction of ROS by hydrogen in type I allergy is the consequence of inhibition of signal transduction, but not of direct radical scavenging activity.

Based on these findings, we hypothesized that hydrogen may ameliorate a wide variety of diseases, irrespective of their causal association with oxidative stress, through modulating yet

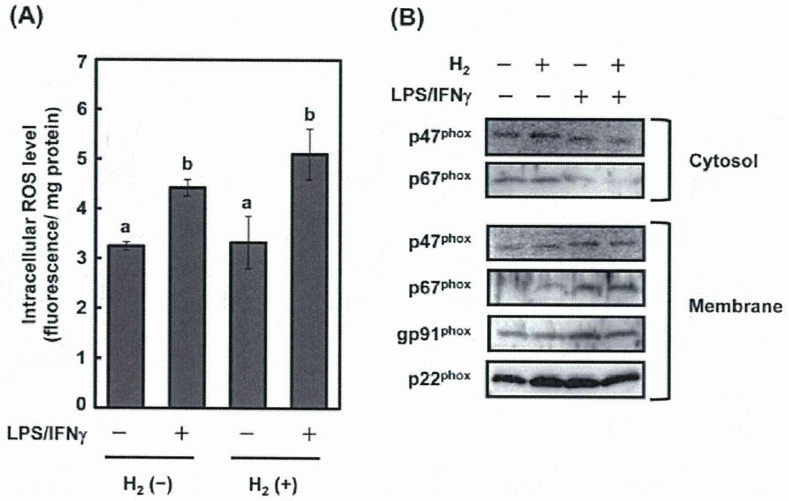

Fig. 3. Effects of hydrogen on LPS/IFNγ-induced NOX activation and ROS production in RAW264 macrophage cells. RAW264 macrophage cells were incubated for 24 h in the presence or absence of hydrogen. (A) Cells were incubated with 10 μM CM-H_2DCF-DA for 1 h in PBS and then treated with or without LPS/IFNγ. Three hours after incubation in the presence or absence of hydrogen, cell lysates were harvested and subjected to measurement of intracellular ROS (mean ± SD, $n = 6$). Statistical significance was determined by two-way ANOVA and Fisher's multiple range test ($p < 0.05$). (B) Cells were treated with or without LPS/IFNγ and then cultured in the presence or absence of hydrogen. Three hours later, the cytosolic and membrane fractions were separated and subjected to Western blot analysis for indicated proteins. A representative blot from three independent experiments is shown.

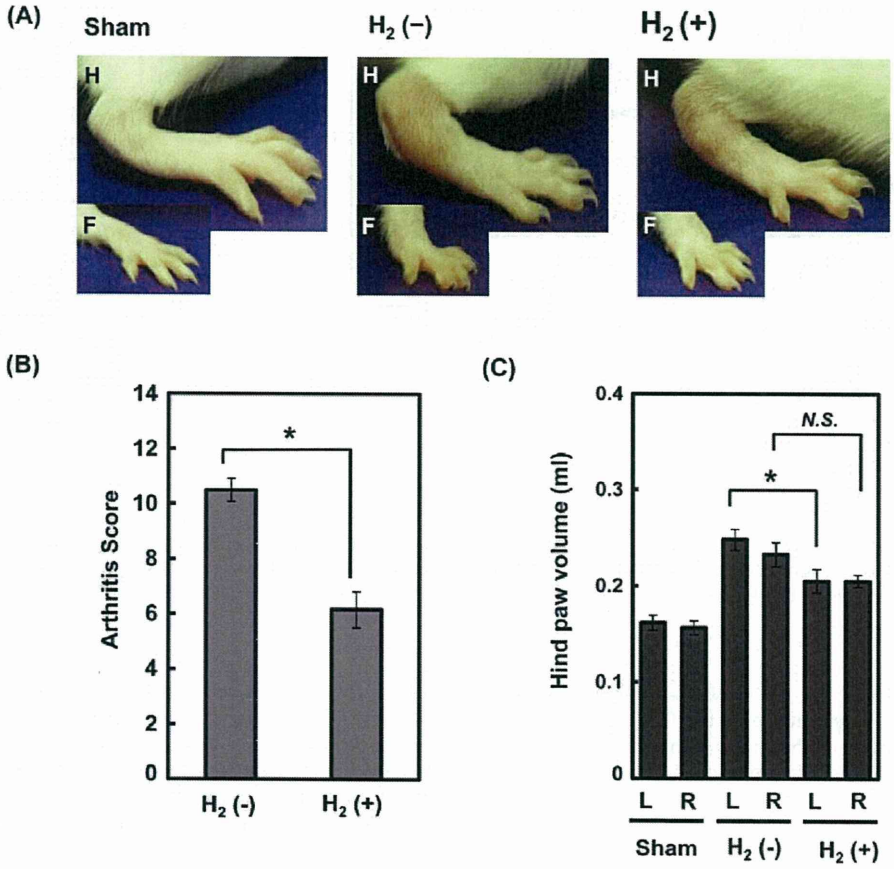

Fig. 4. Effects of oral intake of hydrogen-rich water on anti-type II collagen antibody-induced arthritis in mice. After treatment with or without hydrogen for 2 weeks, BALB/c Cr Slc female mice were injected intravenously with 1 mg of the arthritogenic mouse monoclonal anti-type II collagen antibody cocktail. Three days later, 25 μg of LPS was injected intraperitoneally. Two weeks after the antibody injection, photographs of the hind and front paws were taken (A), the arthritis score was evaluated (B), and the foot volume of hind paws was measured using the plethysmometer (C). Values are expressed as mean ± SD ($n = 5$). Asterisks indicate statistical significance as determined by Student's t-test (*$p < 0.05$). N.S., not statistically significant; L, left; R, right.

unidentified signaling pathways and also that hydrogen may functionally interact with other gaseous signaling molecule, NO, carbon monoxide (CO) and hydrogen sulfide (H_2S). In an attempt to corroborate our hypotheses, we focused on inflammation because of the following reasons. First, it has been reported that hydrogen alleviates several inflammatory diseases [10,11], the mechanism of which, however, remains unknown. Second, in the inflammatory processes, LPS/IFNγ-induced activation of signal transduction leads to expression of iNOS, resulting in up-regulation of NO.

In the present study, we demonstrated that hydrogen suppresses LPS/IFNγ-induced NO release from macrophage cells (Fig. 1A), which was due to inhibition of LPS/IFNγ-induced expression of iNOS (Fig. 1B and C). We also revealed that LPS/IFNγ-induced phosphorylation of p38, JNK and IκBα was specifically suppressed by hydrogen (Fig. 2A and B). These results suggest that hydrogen may reduce binding to the iNOS promoter of several transcription factors such as AP1 and NFκB via inhibition of signal transduction.

Since our results showed that LPS/IFNγ-induced activation of p38 and JNK is inhibited by hydrogen, we investigated the effects of hydrogen on phosphorylation of ASK1, which is an upstream signaling molecule of both kinases [13]. Indeed, ASK1 phosphorylation was inhibited by hydrogen (Fig. 2C). We also asked if hydrogen directly inhibits phosphorylation of ASK1 *in vitro*, but found that ASK1 phosphorylation is not changed by the presence of hydrogen (Supplementary Fig. 1). On the other hand, ROS-dependent activation of the TRAF6–ASK1–p38 pathway is selectively required for TLR4-mediated innate immunity [15]. In addition, ASK1 is an important effector of NOX in the redox signaling [16]. We thus examined the effects of hydrogen on LPS/IFNγ-induced activation of NOX and subsequent production of ROS, but neither of them was affected by hydrogen treatment (Fig. 3).

In addition to ASK1, hydrogen strongly inhibited the NFκB signaling (Fig. 2B) as represented by a marked decrease in LPS/IFNγ-induced expression of COX2 as well as iNOS (Fig. 1B). In TLR4 signaling, LPS induces interaction of TLR4 with TRAF6, an E3 ubiquitin–protein ligase, and promotes TRAF6 auto-ubiquitination, leading to ubiquitination and activation of TAK1 [18]. TAK1 phosphorylates IκB kinases, which in turn phosphorylate IκB, resulting in IκB degradation and NFκB translocation into the nucleus. TAK1 also activates JNK and p38 MAP kinases by phosphorylating MKK4/7 and MKK3/6, respectively. We therefore investigated if hydrogen could inhibit LPS/IFNγ-induced phosphorylation of TAK1, but TAK1 activation was not affected by treatment with hydrogen (Fig. 2C).

Taken together, we demonstrated that hydrogen inhibits LPS/IFNγ-induced phosphorylation of ASK1 and its downstream signaling molecules (p38 and JNK) as well as IκBα in macrophage cells. Although we were unable to identify the exact molecule(s) that hydrogen directly modulates, we could narrow down the potential target sites. In TLR4 signaling, after formation of the LPS/CD14/TLR4 ligand receptor complex, MyD88 and IRAK as well as TRAF6 and TAK1 are recruited, and their interaction mediates downstream signaling. Our studies suggest that hydrogen modulates molecular events at the receptor or immediately downstream of it. In type I allergy, although the presence of the feed-forward loop in the FcεRI-mediated signal transduction prevented us from identifying direct target(s) of hydrogen, we proposed as a plausible mechanism that hydrogen may compromise the initial step of signal transduction, phosphorylation of Lyn kinase [3]. Together with the findings from the present studies, it is tempting to speculate that molecular hydrogen acts at or around the receptors. Nevertheless, the hypothesis remains to be proved by further studies.

In cultured macrophage cells, we showed that hydrogen inhibits TLR4 signaling that plays a critical role in induction of pro-inflammatory genes, providing the molecular bases for the hydrogen effects on inflammatory diseases. Finally, we studied *in vivo* effects of hydrogen on inflammation using a mouse model for human rheumatoid arthritis. It was found that oral intake of hydrogen-rich water suppresses inflammation and ameliorates anti-type II collagen antibody-induced arthritis (Fig. 4). Although we and others have demonstrated beneficial effects of hydrogen on inflammatory diseases in animal models, its efficacy in humans needs to be established in clinical trials.

We confirmed that hydrogen is capable of modulating signal transduction and suggested a role for molecular hydrogen as a signal modulator. Since a number of functional interactions among NO, CO and H_2S have been reported [19], it is conceivable that hydrogen may interact with other gas molecules. Indeed, we demonstrated a functional interaction between NO and hydrogen and elucidated the underlying mechanisms. Future studies will provide information about interactions among four gaseous signaling molecules and their physiological significance.

Competing interest statement

The authors declare no conflict of interest.

Acknowledgments

This work was supported by Grant for Biological Research from Gifu prefecture, Japan (Masafumi Ito) and Grants-in-Aid from the Ministry of Education, Culture, Sports, Science, and Technology, Japan (Masafumi Ito).

Appendix A. Supplementary data

Supplementary data associated with this article can be found, in the online version, at doi:10.1016/j.bbrc.2011.06.116.

References

[1] S. Ohta, A. Nakao, K. Ohno, The 2011 Medical Molecular Hydrogen Symposium: An inaugural symposium of the journal Medical Gas Research, Med. Gas Res. 1 (2011) 10.
[2] I. Ohsawa, M. Ishikawa, K. Takahashi, M. Watanabe, K. Nishimaki, K. Yamagata, K. Katsura, Y. Katayama, S. Asoh, S. Ohta, Hydrogen acts as a therapeutic antioxidant by selectively reducing cytotoxic oxygen radicals, Nat. Med. 13 (2007) 688–694.
[3] T. Itoh, Y. Fujita, M. Ito, A. Masuda, K. Ohno, M. Ichihara, T. Kojima, Y. Nozawa, M. Ito, Molecular hydrogen suppresses FcepsilonRI-mediated signal transduction and prevents degranulation of mast cells, Biochem. Biophys. Res. Commun. 389 (2009) 651–656.
[4] C. Bogdan, Nitric oxide and the immune response, Nat. Immunol. 2 (2001) 907–916.
[5] S.B. Abramson, A.R. Amin, R.M. Clancy, M. Attur, The role of nitric oxide in tissue destruction, Best Pract. Res. Clin. Rheumatol. 15 (2001) 831–845.
[6] M.A. Gassull, Review article: the role of nutrition in the treatment of inflammatory bowel disease, Aliment. Pharmacol. Ther. 20 (Suppl. 4) (2004) 79–83.
[7] C. Nathan, Q.W. Xie, Regulation of biosynthesis of nitric oxide, J. Biol. Chem. 269 (1994) 13725–13728.
[8] E.D. Chan, D.W. Riches, IFN-gamma + LPS induction of iNOS is modulated by ERK, JNK/SAPK, and p38(mapk) in a mouse macrophage cell line, Am. J. Physiol. Cell Physiol. 280 (2001) C441–C450.
[9] A.T. Jacobs, L.J. Ignarro, Lipopolysaccharide-induced expression of interferon-beta mediates the timing of inducible nitric-oxide synthase induction in RAW 264.7 macrophages, J. Biol. Chem. 276 (2001) 47950–47957.
[10] K. Xie, Y. Yu, Z. Zhang, W. Liu, Y. Pei, L. Xiong, L. Hou, G. Wang, Hydrogen gas improves survival rate and organ damage in zymosan-induced generalized inflammation model, Shock 34 (2010) 495–501.
[11] M. Kajiya, M.J. Silva, K. Sato, K. Ouhara, T. Kawai, Hydrogen mediates suppression of colon inflammation induced by dextran sodium sulfate, Biochem. Biophys. Res. Commun. 386 (2009) 11–15.
[12] E. Douni, P.P. Sfikakis, S. Haralambous, P. Fernandes, G. Kollias, Attenuation of inflammatory polyarthritis in TNF transgenic mice by diacerein: comparative analysis with dexamethasone, methotrexate and anti-TNF protocols, Arthritis Res. Ther. 6 (2004) R65–R72.
[13] H. Nagai, T. Noguchi, K. Takeda, H. Ichijo, Pathophysiological roles of ASK1-MAP kinase signaling pathways, J. Biochem. Mol. Biol. 40 (2007) 1–6.
[14] M. Landstrom, The TAK1–TRAF6 signalling pathway, Int. J. Biochem. Cell Biol. 42 (2010) 585–589.

[15] A. Matsuzawa, K. Saegusa, T. Noguchi, C. Sadamitsu, H. Nishitoh, S. Nagai, S. Koyasu, K. Matsumoto, K. Takeda, H. Ichijo, ROS-dependent activation of the TRAF6–ASK1–p38 pathway is selectively required for TLR4-mediated innate immunity, Nat. Immunol. 6 (2005) 587–592.
[16] F. Jiang, Y. Zhang, G.J. Dusting, NADPH oxidase-mediated redox signaling: roles in cellular stress response, stress tolerance, and tissue repair, Pharmacol. Rev. 63 (2011) 218–242.
[17] K. Terato, D.S. Harper, M.M. Griffiths, D.L. Hasty, X.J. Ye, M.A. Cremer, J.M. Seyer, Collagen-induced arthritis in mice: synergistic effect of *E. coli* lipopolysaccharide bypasses epitope specificity in the induction of arthritis with monoclonal antibodies to type II collagen, Autoimmunity 22 (1995) 137–147.
[18] C. Wang, L. Deng, M. Hong, G.R. Akkaraju, J. Inoue, Z.J. Chen, TAK1 is a ubiquitin-dependent kinase of MKK and IKK, Nature 412 (2001) 346–351.
[19] M. Kajimura, R. Fukuda, R.M. Bateman, T. Yamamoto, M. Suematsu, Interactions of multiple gas-transducing systems: hallmarks and uncertainties of CO, NO, and H_2S gas biology, Antioxid. Redox Signal. 13 (2010) 157–192.

Ito et al. Medical Gas Research 2011, 1:24
http://www.medicalgasresearch.com/content/1/1/24

MEDICAL GAS RESEARCH

RESEARCH Open Access

Open-label trial and randomized, double-blind, placebo-controlled, crossover trial of hydrogen-enriched water for mitochondrial and inflammatory myopathies

Mikako Ito[1†], Tohru Ibi[2†], Ko Sahashi[3], Masashi Ichihara[4], Masafumi Ito[5] and Kinji Ohno[1*]

Abstract

Background: Molecular hydrogen has prominent effects on more than 30 animal models especially of oxidative stress-mediated diseases and inflammatory diseases. In addition, hydrogen effects on humans have been reported in diabetes mellitus type 2, hemodialysis, metabolic syndrome, radiotherapy for liver cancer, and brain stem infarction. Hydrogen effects are ascribed to specific radical-scavenging activities that eliminate hydroxyl radical and peroxynitrite, and also to signal-modulating activities, but the detailed molecular mechanisms still remain elusive. Hydrogen is a safe molecule that is largely produced by intestinal bacteria in rodents and humans, and no adverse effects have been documented.

Methods: We performed open-label trial of drinking 1.0 liter per day of hydrogen-enriched water for 12 weeks in five patients with progressive muscular dystrophy (PMD), four patients with polymyositis/dermatomyositis (PM/DM), and five patients with mitochondrial myopathies (MM), and measured 18 serum parameters as well as urinary 8-isoprostane every 4 weeks. We next conducted randomized, double-blind, placebo-controlled, crossover trial of 0.5 liter per day of hydrogen-enriched water or placebo water for 8 weeks in 10 patients with DM and 12 patients with MM, and measured 18 serum parameters every 4 weeks.

Results: In the open-label trial, no objective improvement or worsening of clinical symptoms was observed. We, however, observed significant effects in lactate-to-pyruvate ratios in PMD and MM, fasting blood glucose in PMD, serum matrix metalloproteinase-3 (MMP3) in PM/DM, and serum triglycerides in PM/DM. In the double-blind trial, no objective clinical effects were observed, but a significant improvement was detected in lactate in MM. Lactate-to-pyruvate ratios in MM and MMP3 in DM also exhibited favorable responses but without statistical significance. No adverse effect was observed in either trial except for hypoglycemic episodes in an insulin-treated MELAS patient, which subsided by reducing the insulin dose.

Conclusions: Hydrogen-enriched water improves mitochondrial dysfunction in MM and inflammatory processes in PM/DM. Less prominent effects with the double-blind trial compared to the open-label trial were likely due to a lower amount of administered hydrogen and a shorter observation period, which implies a threshold effect or a dose-response effect of hydrogen.

* Correspondence: ohnok@med.nagoya-u.ac.jp
† Contributed equally
[1]Division of Neurogenetics, Center for Neurological Diseases and Cancer, Nagoya University Graduate School of Medicine, 65 Tsurumai, Showa-ku, Nagoya 466-8550, Japan
Full list of author information is available at the end of the article

Background

Ohsawa and colleagues first reported an effect of hydrogen gas on cerebral infarction in June 2007 [1]. Effects of hydrogen administered in the forms of inhaled gas, drinking water, instillation, and intraperitoneal injection have been reported for 31, 4, and 5 diseases in animal models, cells, and humans, respectively [2]. Hydrogen exhibits prominent effects especially on oxidative stress-mediated diseases and inflammatory diseases in rodents. Hydrogen scavenges hydroxyl radicals and less efficiently peroxynitrite [1]. The radical-scavenging activities, however, are unlikely to be an exclusive mechanism, because the amount of radical oxygen species generated in rodents and humans is much more than the amount of hydrogen molecules taken up by the body. Indeed, the amount of hydrogen taken up by drinking hydrogen-enriched water (HEW) is 100 or more times less than that by inhaling 2% hydrogen gas, but drinking HEW exhibits beneficial effects as good as or even better than inhaling 2% hydrogen gas in rodents [2-4], which suggests the lack of a simple dose-response effect. Our previous study on type 1 allergy also indicates that hydrogen suppresses type 1 allergy by acting as a gaseous signal modulator not as a radical scavenger [5].

Effects of hydrogen in humans have been examined in five studies. First, a randomized, double-blind, placebo-controlled crossover study of 900 ml/day of HEW for 8 weeks in 30 patients with diabetes mellitus type 2 demonstrated significant decreases of electronegative charge-modified LDL cholesterol, small dense LDL, and urinary 8-isoprostanes [6]. Second, an open-label trial of electrolyzed hydrogen-enriched hemodialysis solution in 9 patients for 4 months [7] and 21 patients for 6 months [8] showed significant decreases of systolic blood pressure before and after dialysis, as well as of plasma monocyte chemoattractant protein 1 and myeloperoxidase. Third, an open-label trial of 1.5-2.0 liters per day of HEW for 8 weeks in 20 subjects with metabolic syndrome exhibited a 39% increase of urinary superoxide dismutase (SOD), a 43% decrease of urinary thiobarbituric acid reactive substances (TBARS), an 8% increase of high density lipoprotein (HDL)-cholesterol, and a 13% decrease of total cholesterol/HDL-cholesterol ratio [9]. Fourth, a randomized placebo-controlled study of 1.5-2.2 liters/day of HEW for 6 weeks in 49 patients receiving radiotherapy for malignant liver tumors showed marked improvements of QOL scores [10]. As the study was not blinded, subjective QOL scores tended to be overestimated by a placebo effect, but objective markers for oxidative stress were also significantly decreased. Fifth, drip infusion of hydrogen-enriched saline in combination with Edaravone, a clinically approved radical scavenger for cerebral infarction, for 7 days in 8 patients with brain stem infarction was compared to 24 such patients receiving Edaravone alone [11]. Although the study was not randomized and not blinded, MRI markers of patients infused with hydrogen showed significant improvements and accelerated normalization.

Being prompted by the prominent effects of hydrogen on inflammatory diseases and oxidative stress-mediated diseases especially in rodents, we performed an open-label trial of drinking 1.0 liter per day of HEW for 12 weeks in 14 patients with muscle diseases, and identified improvement in four parameters: (i) a decrease of the lactate-to-pyruvate ratio in mitochondrial myopathies (MM) and progressive muscular dystrophy (PMD); (ii) a decrease of serum matrix metalloproteinase-3 (MMP3) in polymyositis/dermatomyositis (PM/DM), (iii) a decrease of fasting glucose in PMD, and (iv) a decrease of serum triglycerides in PM/DM. We then conducted a randomized, double-blind, placebo-controlled, crossover trial of 0.5 liter per day of HEW for 8 weeks in 12 MM and 10 DM cases. We observed that HEW significantly improved serum lactate in MM. In both studies, some patients reported subjective improvement of fatigability, diarrhea, and myalgia, but others reported floating sensation and worsening of diarrhea. We observed no objective improvement or worsening of clinical symptoms during each study. Our studies imply that HEW improves clinical parameters in MM and PM/DM, but 0.5 liter/day for 8 weeks is likely to be insufficient to demonstrate statistically significant effects.

Patients and methods

Patients

For the open-label trial, we recruited 5 patients with PMD, 4 patients with PM/DM, and 5 patients with MM. The PMD patients comprised 1 male with Miyoshi myopathy and 4 females with limb girdle muscular dystrophy type 2B with an average age and SD of 50.4 ± 15.9 years (range 25 - 66). The PM/DM patients comprised 2 males and 2 females with an average age of 53.8 ± 24.8 years (range 29 - 83). All the PM/DM cases were taking 5 - 10 mg of prednisolone per day and were well controlled. The MM patients comprised 4 cases with MELAS (2 males and 2 females with an average age of 45.8 ± 12.3 years, range 37 - 64) and a 54-year-old female with chronic progressive external ophthalmoplegia (CPEO).

For the randomized, double-blind, placebo-controlled, crossover trial, we recruited 12 patients with MM and 10 patients with DM. The MM patients comprised 5 cases with MELAS (2 males and 3 females with an average age of 44.6 ± 17.6 years, range 20 - 65), as well as 7 cases with CPEO (3 males and 4 females with an average age of 49.1 ± 11.1 years, range 29 - 61). The DM patients comprised 3 males and 7 females with an

average age of 49.6 ± 13.7 years (range 32 - 66). All the DM patients were well controlled with 5 - 10 mg prednisolone per day. Three MM and three DM patients participated in both trials. Both trials were approved by the Ethical Review Board of the Aichi Medical University. Informed consent was obtained from each patient.

Protocols

We purchased 500 ml HEW or placebo water in aluminum pouch from Blue Mercury Inc. (Tokyo, Japan). We measured hydrogen concentrations using an H2-N hydrogen needle sensor attached to a PA2000 2-Channel Picoammeter (Unisense Science, Aarhus, Denmark). The hydrogen concentrations were ~0.5 ppm (~31% saturation). We also confirmed that hydrogen in placebo water was undetectable with our system. For each trial, we instructed patients to evacuate the air from the pouch and to close a plastic cap tightly every time after they drink water to keep the hydrogen concentration as high as possible.

For the open-label trial, patients took 1.0 liter per day of HEW in five to ten divided doses for 12 weeks. We measured 18 serum and one urinary parameters and recorded clinical symptoms at 0, 4, 8, 12, 16 weeks.

For the double-blind trial, patients took 0.5 liter per day of HEW or placebo water in two to five divided doses for 8 weeks. Between the 8-week trials with HEW and placebo, we placed a 4-week washout period. We measured 18 serum parameters and recorded clinical symptoms at 0, 4, 8, 12, 16, 20, 24 weeks. In the double-blind trial, we did not measure urinary 8-isoprostane levels.

The data were statistically analyzed using one-way repeated measures ANOVA for the open-label trial and two-way repeated measures ANOVA for the double-blind trial, both followed by the Bonferroni's multiple comparison test using Prism version 4.0c (Graphpad Software, San Diego, CA).

Results

Open-label trial

Fourteen patients with PMD, PM/DM, and MM participated in the study and no patient dropped out of the study. Patients took 1.0 liter of HEW for 12 weeks and we measured 18 serum and one urinary parameters every 4 weeks (Table 1). We observed no objective improvement or worsening of clinical symptoms during the study. All the patients reported increased micturition frequency. Two MELAS patients reported improvement of fatigability, and another MELAS patient complained mild occasional floating sensation. We estimated statistical significance using one-way repeated measures ANOVA analysis and detected five parameters (Figure 1). Serum lactate-to-pyruvate (L/P) ratios of MM patients were high before the study, and were decreased during the study (Figure 1A). Serum L/P ratios and fasting glucose levels of PMD patients were elevated after the study, but the values were still within normal ranges (Figures 1B and 1C). Serum MMP3 levels of DM patients were decreased down to 72.9% of those before HEW, which were again increased after the study (Figure 1D). Serum triglyceride levels of DM patients were elevated after the study (Figure 1E).

Randomized, double-blind, placebo-controlled, crossover trial

Twelve MM and ten DM patients participated in the study and no patient dropped out of the study. Patients took 0.5 liter of HEW or placebo water for 8 weeks and we measured 18 serum parameters every 4 weeks (Table 2). An MM patient reported increased micturition frequency on HEW. A DM patient reported subjective improvement of fatigability and diarrhea on HEW, but an MM patient rather complained increased diarrhea at first on HEW. Another DM patient reported an improvement of myalgia on HEW. A MELAS patient had hypoglycemic episodes only on HEW, but the episodes subsided after the insulin dose was decreased. We observed no objective improvement or worsening of clinical symptoms during the study. Two-way repeated measures ANOVA analysis revealed that only serum lactate levels were significantly decreased in MM by HEW (Figure 2A). Temporal profiles of serum L/P ratios in MM (Figure 2B) and of serum MMP3 levels in DM (Figure 2C) also demonstrated favorable responses to HEW but without statistical significance.

Discussion

We performed open-label and double-blind studies of HEW on myopathic patients. In the open-label study, we observed statistical significance of hydrogen effects in four parameters: L/P ratios in MM and PMD; fasting glucose in PMD; MMP3 in PM/DM; and triglycerides in PM/DM (Figure 1). In the double-blind study, serum lactate levels were significantly improved in MM. L/P ratios in MM and MMP3 in DM were also improved but without statistical significance (Figure 2). Small numbers of participants in both the open-label and double-blind studies might have failed to disclose statistically significant effects of HEW.

In MM, the mitochondrial electron transfer system (mETS) is compromised by mutations in mitochondrial DNA [12]. This results in a decreased influx of NADH into mETS and elevates NADH levels in the cytoplasm, which facilitates conversion of pyruvate to lactate by lactate dehydrogenase. Thus, lactate and L/P ratio are useful surrogate markers to estimate functions of mETS, and are usually abnormally elevated in MM [12]. Defective mETS also causes leakage of electrons from

Table 1 Open-label trial of HEW in 14 myopathic patients

	Progressive muscular dystrophy (PMD)			Polymyositis (PM)/Dermatomyositis (DM)			Mitochondrial myopathies (MM)		
	Before	12 weeks	After	Before	12 weeks	After	Before	12 weeks	After
CK (U/L)	3067 ± 1492	3419 ± 1610	3107 ± 2382	124 ± 31	180 ± 97	140 ± 86	187 ± 75	124 ± 47	156 ± 40
HbA1c (%)	5.25 ± 0.44	5.14 ± 0.31	5.16 ± 0.42	6.68 ± 1.61	6.70 ± 1.53	6.90 ± 2.03	7.40 ± 1.70	7.32 ± 1.48	7.38 ± 1.74
Fasting glucose (mmol/L)	5.52 ± 0.16**	5.51 ± 0.08**	5.82 ± 0.11**	7.66 ± 0.11	7.29 ± 1.57	7.69 ± 1.85	8.94 ± 3.24	9.31 ± 4.18	8.96 ± 3.19
Lactate (mmol/L)	0.95 ± 0.34	1.15 ± 0.40	1.35 ± 0.40	1.42 ± 0.18	1.66 ± 0.32	1.30 ± 0.27	1.84 ± 0.50	1.87 ± 0.78	1.73 ± 0.65
L/P ratio	12.1 ± 0.7*	10.7 ± 1.3*	13.6 ± 2.2*	13.1 ± 0.9	15.0 ± 3.2	12.7 ± 1.0	20.7 ± 2.9*	14.9 ± 3.5*	20.3 ± 3.1*
Creatinine (μmol/L)	34.8 ± 3.1	34.5 ± 6.9	34.7 ± 8.8	58.6 ± 13.7	56.3 ± 10.7	56.6 ± 14.1	48.8 ± 9.0	47.7 ± 9.7	48.6 ± 8.8
BUN (mmol/L)	4.74 ± 1.16	4.20 ± 0.60	4.21 ± 1.05	4.33 ± 0.71	4.11 ± 0.48	4.68 ± 0.74	5.28 ± 1.69	5.89 ± 1.09	5.00 ± 1.58
Uric acid (μmol/dL)	295 ± 46	315 ± 61	300 ± 30	319 ± 44	331 ± 71	329 ± 40	208 ± 50	220 ± 60	217 ± 45
Urinary 8-isoprostane (ng/mg Cr)	303 ± 155	392 ± 173	n.d.	222 ± 88	237 ± 86	n.d.	274 ± 117	261 ± 59	n.d.
T-chol (mmol/L)	5.42 ± 0.99	5.74 ± 1.02	5.70 ± 0.81	5.28 ± 0.31	5.55 ± 0.93	5.97 ± 1.35	4.52 ± 0.75	4.53 ± 0.34	4.42 ± 0.77
LDL-chol (mmol/L)	3.30 ± 1.05	2.86 ± 1.46	2.99 ± 1.15	2.66 ± 0.28	3.21 ± 0.99	3.13 ± 1.02	2.44 ± 0.43	2.27 ± 0.44	2.22 ± 0.45
HDL-chol (mmol/L)	1.62 ± 0.21	1.49 ± 0.19	1.62 ± 0.18	2.01 ± 0.73	1.99 ± 0.76	2.02 ± 0.67	1.14 ± 0.79	1.03 ± 0.72	1.04 ± 0.69
Triglycerides (mmol/L)	1.31 ± 0.46	3.62 ± 4.83	3.07 ± 3.67	2.17 ± 0.63*	2.01 ± 1.21*	3.09 ± 1.22*	0.78 ± 0.34	0.89 ± 0.45	0.73 ± 0.37
WBC (10^9/L)	5.30 ± 1.32	5.40 ± 1.12	4.80 ± 0.38	10.78 ± 2.08	8.35 ± 3.41	10.10 ± 0.17	5.12 ± 1.27	7.27 ± 2.29	5.93 ± 1.35
RBC (10^{12}/L)	4.17 ± 0.64	3.79 ± 0.42	3.87 ± 0.80	4.01 ± 0.62	4.34 ± 0.36	4.49 ± 0.45	4.33 ± 0.43	4.31 ± 0.78	4.35 ± 0.59
Platelets (10^9/L)	262 ± 42	260 ± 33	270 ± 20	337 ± 123	265 ± 82	270 ± 65	215 ± 25	207 ± 28	217 ± 25
Hematocrit	0.375 ± 0.040	0.374 ± 0.038	0.407 ± 0.055	0.337 ± 0.069	0.376 ± 0.041	0.395 ± 0.045	0.381 ± 0.036	0.370 ± 0.047	0.378 ± 0.038
MMP3 (ng/ml)	n.d.	n.d.	n.d.	307.8 ± 59.1*	224.3 ± 53.4*	283.3 ± 77.6*	n.d.	n.d.	n.d.
IgG (mg/dl)	n.d.	n.d.	n.d.	1343 ± 470	1396 ± 550	1429 ± 581	n.d.	n.d.	n.d.

Values represent mean ± SD. n.d., not determined. *$p < 0.05$ and **$p < 0.005$ by one-way repeated measures ANOVA.

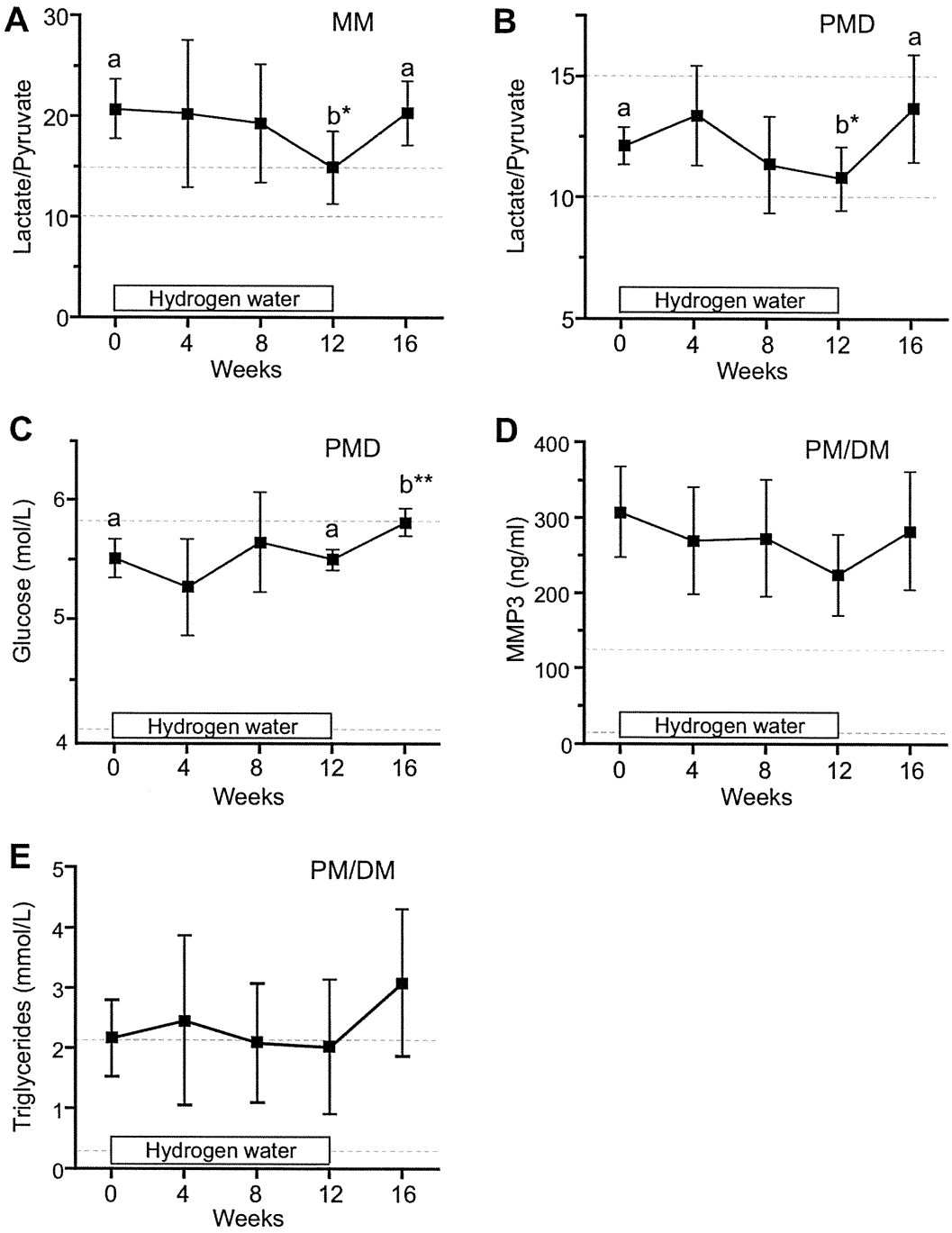

Figure 1 Temporal profiles of four parameters that demonstrate statistical significance by one-way repeated measures ANOVA in the open-label trial. Ratios of serum lactate/pyruvate (L/P) in 5 mitochondrial myopathies (MM) patients **(A)** and 4 progressive muscular dystrophy (PMD) patients **(B)**. Note abnormally high L/P ratios in MM patients. **(C)** Fasting glucose in 4 PMD patients. **(D)** Serum MMP3 in 5 Polymyositis (PM)/Dermatomyositis (DM) patients. **(E)** Serum triglycerides in 4 PMD patients. Twelve weeks on HEW are indicated by a box in each panel. Means and SD are plotted. Statistically different values by the Bonferroni's multiple comparison test are indicated by 'a' and 'b' with $*p < 0.05$ and $**p < 0.01$. Bonferroni's test reveal no statistical difference between any two values in **(D)** and **(E)**. Broken lines show a normal range of each parameter.